Naval Surface Warfare Center
Carderock Division
West Bethesda, MD 20817-5700

NSWCCD-61-TR-2022/16 **September 2022**

Platform Integrity Department
Technical Report

Temperature-Dependent Material Property Database for C63200 Nickel-Aluminum Bronze (NAB) Plate

by
Sean M. Orzolek
Charles R. Fisher

Naval Surface Warfare Center
Carderock Division
West Bethesda, MD 20817-5700

NSWCCD-61-TR-2022/16 **September 2022**

Platform Integrity Department

Technical Report

Temperature-Dependent Material Property Database for C63200 Nickel-Aluminum Bronze (NAB) Plate

by

Sean M. Orzolek

Charles R. Fisher

REPORT DOCUMENTATION PAGE

Form Approved
OMB No. 0704-0188

1. REPORT DATE *(DD-MM-YYYY)*	2. REPORT TYPE	3. DATES COVERED *(From - To)*
19-09-2022	Technical Report	FEB 2021 – June 2022

4. TITLE AND SUBTITLE

Temperature-Dependent Material Property Database for C63200 Nickel-Aluminum Bronze (NAB) Plate

5a. CONTRACT NUMBER N/A

5b. GRANT NUMBER N/A

5c. PROGRAM ELEMENT NUMBER N/A

6. AUTHOR(S)

Sean M. Orzolek
Charles R. Fisher

5d. PROJECT NUMBER N/A

5e. TASK NUMBER

5f. WORK UNIT NUMBER

7. PERFORMING ORGANIZATION NAME(S) AND ADDRESS(ES) AND ADDRESS(ES)

Naval Surface Warfare Center, Carderock Division
Code 611
9500 MacArthur Boulevard
West Bethesda, MD 20817-5700

8. PERFORMING ORGANIZATION REPORT NUMBER

NSWCCD-61-TR-2022/16

9. SPONSORING / MONITORING AGENCY NAME(S) AND ADDRESS(ES)

William Mullins
Program Manager, Code 332
Office of Naval Research
Arlington, VA 22217

10. SPONSOR/MONITOR'S ACRONYM(S)

11. SPONSOR/MONITOR'S REPORT NUMBER(S) N/A

12. DISTRIBUTION / AVAILABILITY STATEMENT

DISTRIBUTION A. Approved for public release; distribution unlimited.

13. SUPPLEMENTARY NOTES

14. ABSTRACT:

Nickel-aluminum bronze (NAB) alloys are commonly used for marine applications such as propellers, piping, valves, bearings, and fasteners. These NAB components are conventionally manufactured using both casting techniques and rolling and heat treatment techniques. However, limited information is available regarding the high temperature properties of NAB. The following data descriptor report documents the thermo-physical and thermo-mechanical results for a C63200 wrought plate material. These results will help empower Integrated Computational Materials Engineering (ICME) efforts through the integration with commercial software packages. The raw data, in machine-readable form, are available at the University of Michigan's Materials Commons data repository: https://materialscommons.org/.

15. SUBJECT TERMS

Nickel-Aluminum Bronze, NAB, ICME, C63200, database

16. SECURITY CLASSIFICATION OF: UNCLASSIFIED			17. LIMITATION OF ABSTRACT	18. NUMBER OF PAGES	19a. RESPONSIBLE PERSON
a. REPORT	b. ABSTRACT	c. THIS PAGE			Charles Fisher
UNCLASSIFIED	UNCLASSIFIED	UNCLASSIFIED		36	19b. TELEPHONE NUMBER (301)227-4969

CONTENTS

Page

FIGURES

Page

TABLES

Page

ADMINISTRATIVE INFORMATION

The work described in this report was performed by the Welding, Processing, and Nondestructive Evaluation Branch (Code 611) of the Platform Integrity Department at the Naval Surface Warfare Center, Carderock Division (NSWCCD). The work was funded in FY21-22 by the Office of Naval Research (ONR), Code 332, as part of the *Agile Manufacturing Integrated Computational Materials Engineering (ICME) Toolkit* program, also referred to as "Agile ICME" within this report.

ACKNOWLEDGEMENTS

The authors would like to acknowledge the other members of the Agile ICME program team at NSWCCD working on the nickel-aluminum bronze (NAB) for additive manufacturing (AM) efforts, including Jennifer Semple, Jack Canaday, Matthew Dantin, Cindy Waters, Adam Gershen, Jeff Thurman, John Nasrin, Brian Snyder, and Thad Michael. Justin Norkett is especially thanked for his assistance with understanding the temperature-dependent density calculations. In addition, collaborators at the U.S. Naval Research Laboratory (NRL) on the Agile ICME program working on NAB for AM efforts include David Rowenhorst, John Michopoulos, Andrew Birnbaum, Athanasios Iliopoulos, John Steuben, and Colin Stewart among many others. Special thanks to all collaborators for their advice and contributions throughout the project, including Julie Christodoulou and William Mullins at ONR for their foresight in establishing the path to get this program funded, Jennifer Wolk and Richard Fonda at ONR for their current support, as well as Johnnie DeLoach for his guidance and mentorship in helping establish an ICME-based culture at NSWCCD within the Materials and Manufacturing Division (Division 61).

This page intentionally left blank

EXECUTIVE SUMMARY

Nickel-aluminum bronze (NAB) alloys are commonly used for marine applications such as propellers, piping, valves, bearings, and fasteners. These NAB components are conventionally manufactured using both casting techniques and rolling and heat treatment techniques. However, limited information is available regarding the high temperature properties of NAB. The following data descriptor report documents the thermo-physical and thermo-mechanical results for a C63200 wrought plate material. These results will help empower Integrated Computational Materials Engineering (ICME) efforts through the integration with commercial software packages. The raw data, in machine-readable form, are available at the University of Michigan's Materials Commons data repository: https://materialscommons.org/.

BACKGROUND

The shipbuilding industry has seen great benefits from the use of nickel-aluminum bronze (NAB) alloys, particularly for such applications as propellers, pumps, piping, valves, bearings, and fasteners [1][2]. These alloys have excellent mechanical properties, particularly strength, fatigue life, and toughness [1][2]. NAB alloys also exhibit high corrosion, erosion, and cavitation resistance, which are vital for any material used in seawater applications [1][2][3][4].

NAB alloys are primarily copper (Cu), with substantial alloying additions of nickel (Ni), aluminum (Al), and iron (Fe). At high temperatures, a body centered cubic (BCC) β phase forms, which typically transforms to a face centered cubic (FCC) α phase interspersed with various κ precipitates upon cooling [1][5]. The microstructure of NAB alloys is sensitive to changes in composition as well as to changes in cooling rate, which was described in a recent Naval Surface Warfare Center, Carderock Division (NSWCCD) review on the topic [6]. This review also documented the applications, microstructure, and properties of NAB in detail in regard to various welding and additive manufacturing (AM)-based fabrication techniques. A substantial overview of NAB alloys has been summarized by the Copper Development Association and provides an excellent introduction into other applications and basic properties of NAB alloys [1], which will not be repeated here.

Integrated Computational Materials Engineering (ICME)-based prediction tools can be used to quantify the residual stress and distortion from fabrication, including welding and AM production [7]. Once validated, these tools could be coupled with topology optimization software to mitigate part distortion and minimize cost, weight, or many other factors. These fabrication-based ICME tools require detailed, reliable databases of temperature-dependent material properties to increase the simulation accuracy. Within welded fabrication (or similar wire-based AM processes), of highest importance to the fidelity of such models are the thermo-physical and thermo-mechanical properties of the material(s) being joined. The properties of note include specific heat, thermal conductivity, coefficient of thermal expansion (CTE), elastic modulus, yield strength, and flow stress, from room temperature up to nearly the alloy's melting point. The temperatures associated with on-heating and on-cooling phase transformations and their variation with heating rate, cooling rate, and peak temperature are also important for the prediction of stress and distortion evolution. While this data exist for some of the most common marine-grade steels [8][9][10], the data are sparse for many copper-based alloys, including NAB.

APPROACH

Material Testing Program

The original basis for the material property assessment program was developed through inputs from welding engineers at NSWCCD, researchers at The Ohio State University (OSU), and modeling

experts at ESI for marine-grade high-strength steels [10]. The program focused on generating the types of data required to develop marine-relevant material databases for use by ESI's commercial software, *SYSWELD*. The raw data could also be adapted for use by other finite element analysis (FEA) tools, such as Hexagon's *Simufact Welding* or the welding module for *Abaqus*. Specific data included thermo-physical and thermo-mechanical properties of the alloys of interest, from room temperature up to near-melting, along with other thermo-metallurgical information on microstructural evolution. Density, heat capacity, thermal conductivity, and coefficient of thermal expansion (CTE) were identified as the most important thermo-physical properties. Thermo-mechanical properties of interest included the elastic modulus, yield strength, and flow stress.

The C63200 NAB base plate used in this study was in the form of 2.54 x 20.32 x 31.12 cm (1 x 8 x 12.25 in.) plates purchased from Diversified Metals Incorporated in Monson, MA. Each plate met the criteria of ASTM B150 [11] as shown in **Table 1**. Note that in this specification the measured copper value includes silver, the measured nickel value includes cobalt, and the iron content shall not exceed the nickel content. These plates were heat-treated at 850 °C (1562 °F) for one hour followed by oil quenching, then tempered at 700 °C (1292 °F) for three hours followed by air cooling. The room temperature minimum yield strength, ultimate tensile strength (UTS) range, and minimum elongation requirements for the alloy are 352 MPa (51 ksi), 490 to 621 MPa (71 to 90 ksi), and 19% in 200 mm (8 in.) or 22% in 50 mm (2 in.), respectively [11]. The plate conformance certification sheet from the supplier for the material investigated in this study is given in **Appendix A**. NSWCCD validation of the composition was conducted using glow discharge atomic emission spectrometry (GD-AES) on a Leco GDS900 in accordance with ASTM E415 [12], as shown in **Table 1**. The reported measured value is an average across four tests, with the raw data given in **Appendix B**.

Table 1. Chemical Composition of C63200 NAB Base Plate (wt%)

Element	Al	Fe	Ni (+Co)	Mn	Si*	Sn*	Zn*	Pb*	Cu (+Ag)
Specification [11]	8.7-9.5	3.5-4.3	4.0-4.8	1.2-2.0	<0.10	---	---	<0.02	Bal.
Supplier [Appendix A]	9.25	3.81	4.49	1.35	0.03	0.01	0.02	<0.01	Bal.
Measured Average	9.03	3.85	4.49	1.23	0.033	0.017	0.06	0.003	81.26

** Element not included in JMatPro or Thermo-Calc thermodynamic modeling*

Calculated Phase Diagram (CALPHAD) Modeling

Sente Software's *JMatPro* program (version 13.0) was used with the proprietary Sente Software copper alloy database to predict some of the temperature-dependent thermo-physical and thermo-mechanical properties of the NAB material; namely density, CTE, specific heat capacity, thermal conductivity, and elastic modulus. The liquidus and solidus was also predicted using *JMatPro* based on the phase evolution. Additionally, *Thermo-Calc* (version 2023a) was used with their TCCU5 database to predict the density and specific heat capacity of the NAB material. Other thermo-physical and thermo-mechanical properties were not able to be predicted due to current model limitations in both software packages. All CALPHAD simulations were conducted between 25 and 1200 °C (77 and 2192 °F) using the simplified, NSWCCD-measured composition in **Table 1**, where the trace elements (0.1 wt% and below, as noted in the chart) were not included to prevent erroneous phase predictions.

Thermo-Physical Property Analysis

Solidus and Liquidus Analysis

Dynamic scanning calorimetry (DSC) was conducted at NSWCCD using a SDT Q600 unit with a specimen mass of 30 mg and an argon gas flow of 100 mL/min. Specimens were placed in an alumina crucible and were heated at a rate of 20 °C/min (36 °F/min) up to a peak temperature of 1200 °C (2192 °F) held for one minute and cooled at a rate of 20 °C/min (36 °F/min). The DSC curves revealed the solidus and liquidus temperatures as well as the latent heat of fusion.

Coefficient of Thermal Expansion and Phase Transformation Analysis

Dilatometry was conducted using the Gleeble 3500 at NSWCCD in an argon atmosphere using flat-plate copper grips. The specimens were extracted in the rolling direction and machined into a cylindrical specimen geometry with a length of 70 mm (2.76 in.) and diameter of 3 mm (0.12 in.). The Gleeble operates on the principles of resistive heating, conductive cooling through water-cooled fixturing, and rapid (50 kHz) control system feedback to apply precise thermal cycles. A Keyence LS9120MR laser micrometer was positioned perpendicular to the specimen to measure the expansion of the material. Samples were heated at a rate of 10 °C/s (18 °F/s) to a specified peak temperature, held for five seconds, and free-cooled to ambient temperature.

Testing was initially conducted using the "pocket jaw" setup using stroke control to zero the force. However, due to the low strength of NAB at high temperatures, there was significant compression of the specimen, resulting in a bulging of the sample and an artificial inflation in CTE. To remedy this the "floating jaw setup" was used, which reduced the amount of applied force and reduced the extent of bulging. An original objective of this work was to develop a continuous cooling transformation (CCT) diagram for NAB plate. However, the microstructural transformations produced negligible changes in volume on the Gleeble 3500, inhibiting the development of any CCT diagram. Future work is planned to use ultrasonic inspection techniques coupled with a Gleeble system as an alternative approach to observe the temperature-dependent phase transformations.

Temperature-dependent CTE values were calculated from on-heating data collected during a single dilatometry test. CTE was determined for discrete temperatures by calculating the slope of the dilation-temperature curve in the vicinity of the selected temperatures and normalizing by the diameter of the specimen. The best-fit slope was determined using linear regression, and the diameter of the specimen was taken as the room temperature value (3 mm [0.12 in.]). The specimen diameter at the CTE calculation temperatures was not adjusted to include expansion due to temperature because the dilation magnitudes were so small as to have a negligible effect on the calculated CTE. An interval of ±25 °C (45 °F) was selected for calculating the local slope in order to minimize the effect of noise in the data caused by high sampling rates (*e.g.*, CTE at 400 °C [752 °F] was calculated using the slope of the data in the interval of 375-425 °C [707-797 °F] range). A one-sided interval of 25 °C (45 °F) was used to calculate slope at the upper and lower bounds of the CTE calculation temperatures.

Other Thermo-Physical Properties

Pieces of the NAB baseplate were sent to Thermophysical Properties Research Laboratory, Inc. (TPRL) in West Lafayette, IN and tested to obtain thermal properties necessary to create a material database. These properties included thermal diffusivity (α) and specific heat (c_p) measured at temperatures ranging from 23 to 1000 °C (73 to 1832 °F). To measure thermal diffusivity, the laser flash diffusivity method was used in accordance with ASTM E1461 [13]. Specific heat was measured according to ASTM E1269 [14] using a Perkin-Elmer DSC with sapphire as reference material. As the thermal conductivity (λ) is dependent on the density of the material, the temperature-dependent density (ρ) was calculated using a theoretical cubic volume element under the assumption of isotropic thermal expansion in **Equation 1**:

$$\rho(T) = \frac{\rho_0 V_0}{V(T)} \quad \textbf{(1)}$$

where $\rho(T)$ ≡ Density at temperature T [g/cm^3]
ρ_0 ≡ Room temperature density provided by TPRL [g/cm^3]
V_0 ≡ Room temperature volume of the theoretical cubic element [cm^3]
$V(T)$ ≡ Volume of the theoretical cubic element at temperature T [cm^3]

V_0 was calculated assuming a side length equal to the room temperature width of the dilatometry specimens. This value was chosen because it corresponds to the starting gauge length for the dilatometer used to measure thermal expansion. A theoretical cubic volume element was chosen instead of the actual specimen dimensions to subvert potential complications with measuring dimensions that were not directly measured by the dilatometer (*e.g.*, the effect of thermal gradients on measurement of the specimen's longitudinal expansion). V_T was calculated according to **Equation 2.**

$$V(T) = [w(T)]^3 \quad \textbf{(2)}$$

where $w(T)$ ≡ Dilatometer-measured specimen width at temperature T [cm]

This method allowed calculation of the density at each temperature, through dividing the constant mass by the volume (which was dependent upon the CTE values). The temperature-dependent density was then input into **Equation 3** to calculate thermal conductivity (λ) at discrete temperatures.

$$\lambda = \rho \cdot c_p \cdot \alpha \quad \textbf{(3)}$$

where λ ≡ Thermal conductivity [W/cm-°C]
c_p ≡ Specific heat capacity [J/g-°C]
ρ ≡ Density [g/cm^3]
α ≡ Thermal diffusivity [cm^2/s]

Thermo-Mechanical Property Analysis

Tensile specimens were machined from the NAB plates to obtain elastic modulus, yield strength, UTS, and flow stress as a function of temperature. All specimens were extracted with their length perpendicular to the rolling direction of the plate. On-heating tension testing of the NAB plate material at temperatures between 22 and 900 °C (72 and 1652 °F) was subcontracted to IMR Test Labs in Ithaca, NY. Room temperature testing was performed in accordance with ASTM A370 [15], and elevated temperature testing was performed in accordance with ASTM E21 [16]. Specimens were round bars with a gauge diameter of 12.8 mm (0.505 in.) and a gauge length of 25.4 mm (1 in.) according to ASTM E8 [17]. Testing was performed in strain control mode at target rates of 0.005 min^{-1} prior to yield and 0.05 min^{-1} after yield.

Additional on-heating mechanical properties were measured at NSWCCD using the Gleeble 3500 with a Keyence LS9120MR Micrometer utilizing the double-reduced flat-bar specimen geometry, as shown in **Figure 1**. Tensile tests were conducted using the Gleeble 'Pocket Jaw' setup in an argon atmosphere with reduced contact stainless steel grips used to fixture the specimen in order to reduce the thermal gradient in the gauge section. Specimens were heated to the programmed test temperature at a rate of 10 °C/s (18 °F/s) and pulled to failure at a constant crosshead speed of 6 mm/min (0.24-in./min). The micrometer was oriented along the length of the specimen and measured the distance between two reference points in the gauge section. These posts were welded with 0.25 mm (0.010 in.) diameter platinum thermocouples positioned within 3 mm (0.12 in.) of the center of the specimen. Although the Gleeble measures the stroke and therefore the overall extension of the sample, the benefit of using the laser extensometer is that the measurement of strain is localized to the gauge section and thus more

accurate. However, in initial testing, the reference posts were welded too close to the hot zone of the specimen and as the specimen started necking, the reference posts rotated towards one another, resulting in an incorrect reporting of sample extension. To alleviate this, the reference posts were kept at 3 mm (0.12 in.) on either side of the welded thermocouples in the center of the specimen. Preliminary testing indicated that for this setup, the temperature variation across the initial gauge length was 8 °C (4.4 °F) but worsened to 30 °C (16.7 °F) with increasing test time, as the sample deformed, and gauge length increased.

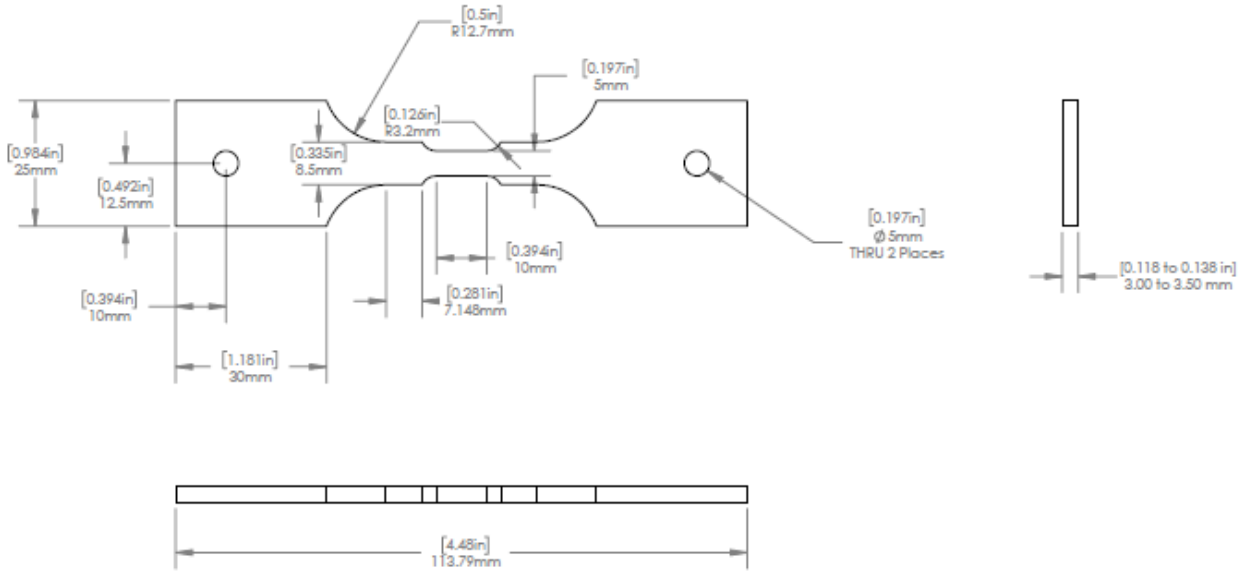

Figure 1. Specimen dimensions for Gleeble-based mechanical testing.

Microstructural Analysis

To quantify and characterize the microstructures observed in NAB, specimens were cross sectioned from the plate material, Gleeble specimens, and DSC specimens for microstructural characterization. Specimens were mounted into a conductive polishing mount and metallographically prepared to a final polish of 0.25 μm using standard techniques followed by etching by 10% Ammonium Persulfate for approximately 14 seconds.

The fracture surface of the tensile specimens was evaluated by stereomicroscopy, light optical microscopy (LOM), and scanning electron microscopy (SEM) analysis. Select specimens were cross-sectioned perpendicular to the fracture surface to reveal the microstructure associated with the elevated temperature tensile testing.

RESULTS AND DISCUSSION

Thermo-Physical Properties

DSC testing revealed the solidification transformations as well as the latent heat of transformation as shown in **Figure 2**. The solidus and liquidus temperature of the primary phase were 1061 °C (1942 °F) and 1086 °C (1987 °F), respectively. The integral of the primary solidification peak on-cooling lead to a measurement of 115.3 J/g for the latent heat of fusion. The predicted solidus and liquidus using the *JMatPro* software was 971 °C (1780 °F) and 1018 °C (1864 °F), respectively, between 68-90 °C (123-162 °F) difference across both values. The microstructural transformation occurring at 990 °C (1814 °F) is likely the transformation of the primary β phase to the two-phase region of $\beta + \alpha$, as suggested by previous studies [18][19].

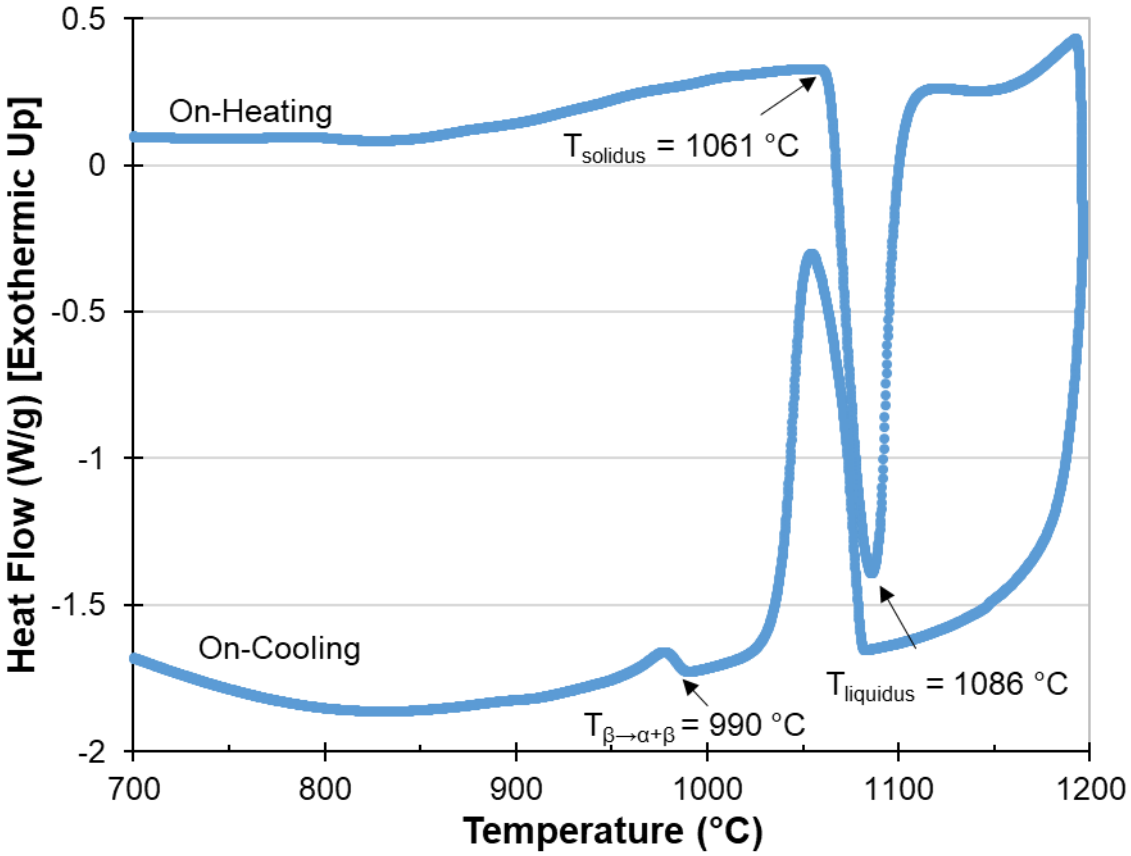

Figure 2. DSC curve of the NAB plate material with labeled phase transformations.

Although NAB exhibits a complex microstructure with a multitude of precipitates and phase transformations occurring on-cooling, these transformations do not result in significant volumetric changes as indicated by the dilatometry curve in **Figure 3**. A slight deviation is observed at ~800 °C (1472 °F) for the on-heating curve, which is likely the $\alpha + \kappa \rightarrow \alpha + \kappa + \beta$ eutectoid transformation as noted in previous work by Hasan *et al.* [19]. However, this change in dilation may also be the result of compressive stresses associated with the uneven heating along the length of the specimen as a result of the resistive heating in the Gleeble system. This would result in a slight bulging in the measured thickness of the sample and is likely why the specimen exhibited an increase in dilation at room temperature. This effect is not apparent in the on-cooling condition, where the cooling rate in air was five times faster (50 °C/s [90 °F/s]).

Therefore, the linear CTE was determined from the on-heating curve only up to 720 °C (1328 °F), and values at increased temperatures (800 °C [1472 °F] and above) were extrapolated from a linear fit of the CTE data between 30-720 °C (86-1328 °F). **Figure 4** shows these data in comparison to values predicted by *JMatPro* simulations. As shown, the predicted values show good agreement with the experimental results at lower temperature and continues the trend until 971 °C (1780 °F), where liquid was predicted to form. This indicates that for the NAB plate alloy, the temperature-dependent CTE in the solid state can be used in future modeling efforts as the predictions are consistent with the experimental results. However, as noted previously, the measured solidus of the NAB plate material was 1061 °C (1942 °F) compared to 971 °C (1780 °F) predicted by *JMatPro*, indicating an inaccuracy in the results near melting and above.

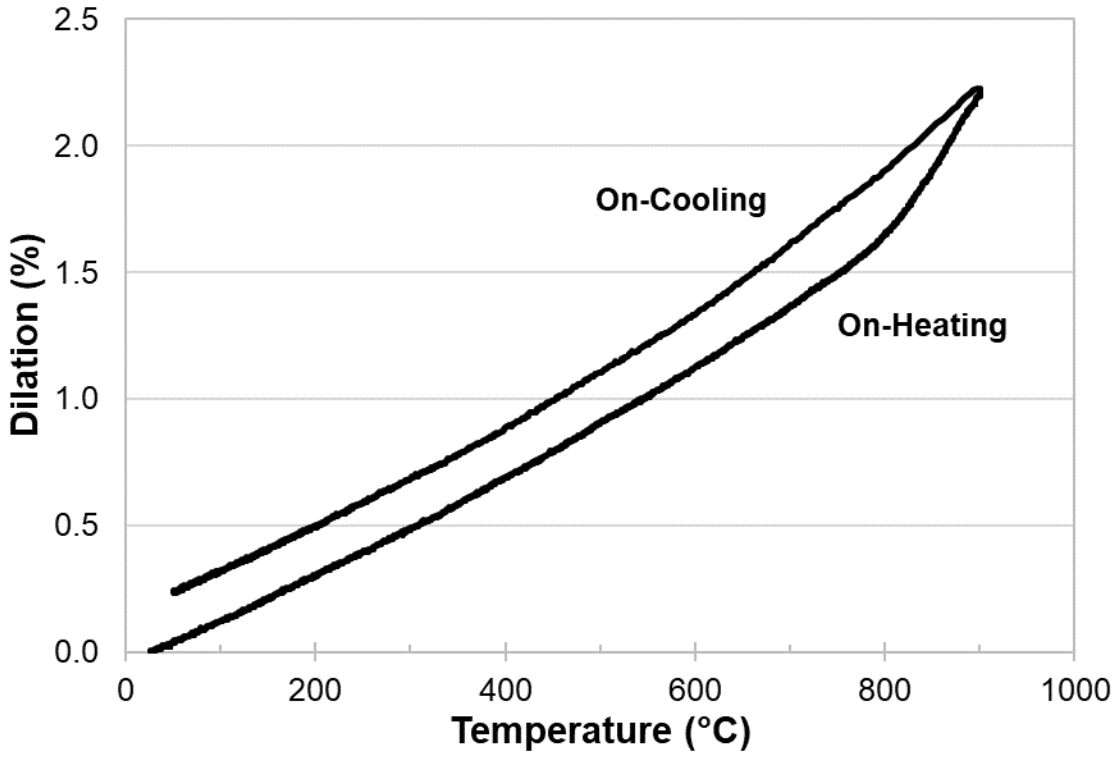

Figure 3. Dilatometry curve of an NAB plate specimen heated at 10 °C/sec to a peak temperature of 900 °C and air cooled.

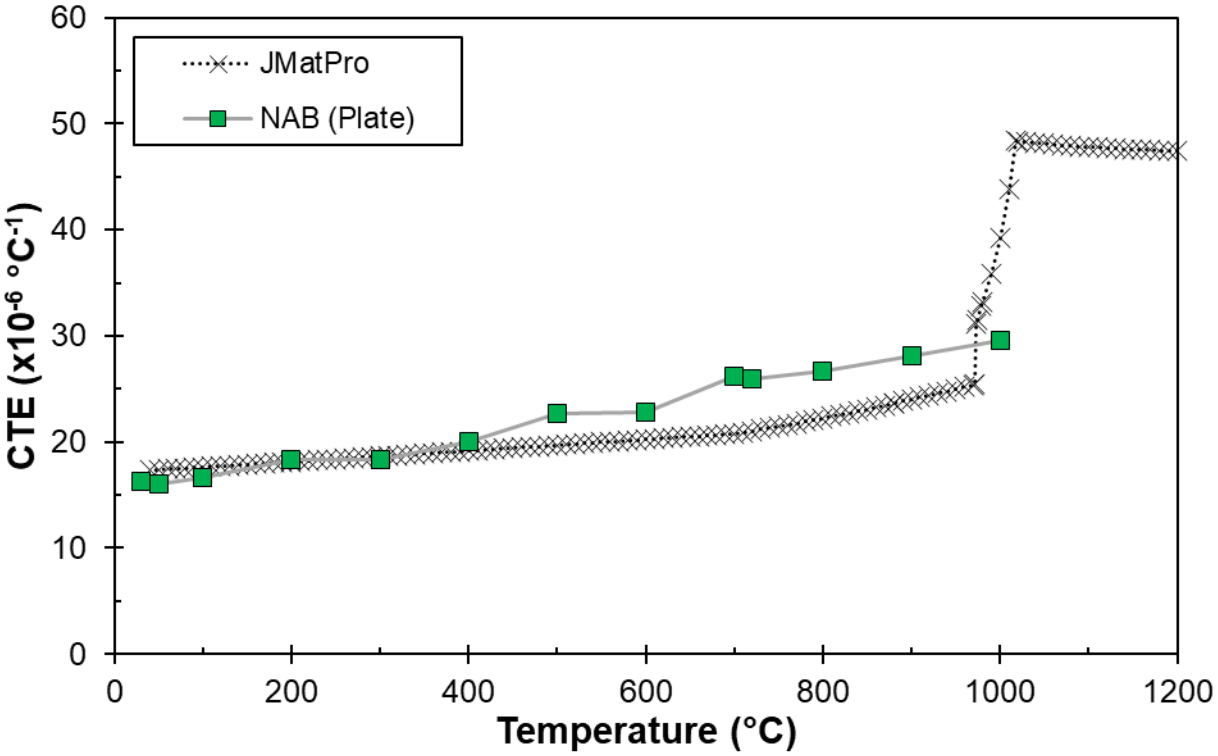

Figure 4. CTE calculated from the on-heating dilatometry curve in **Figure 3** compared to the predicted values from *JMatPro*.

The temperature-dependent density is shown in **Figure 5**, which varied as a function of the CTE. The values match up very closely with the *JMatPro* and *Thermo-Calc* predicted values for much of the measured temperature range. There is a deviation from predicted values around at ~800 °C (1472 °F), likely due to the previously mentioned $\alpha + \kappa \rightarrow \alpha + \kappa + \beta$ transformation which is expected to occur in this temperature range. It should be noted that the 1000 °C (1832 °F) data point of the measured density is extrapolated based on a third order polynomial fit in order to match the range of the thermo-physical data produced by TPRL.

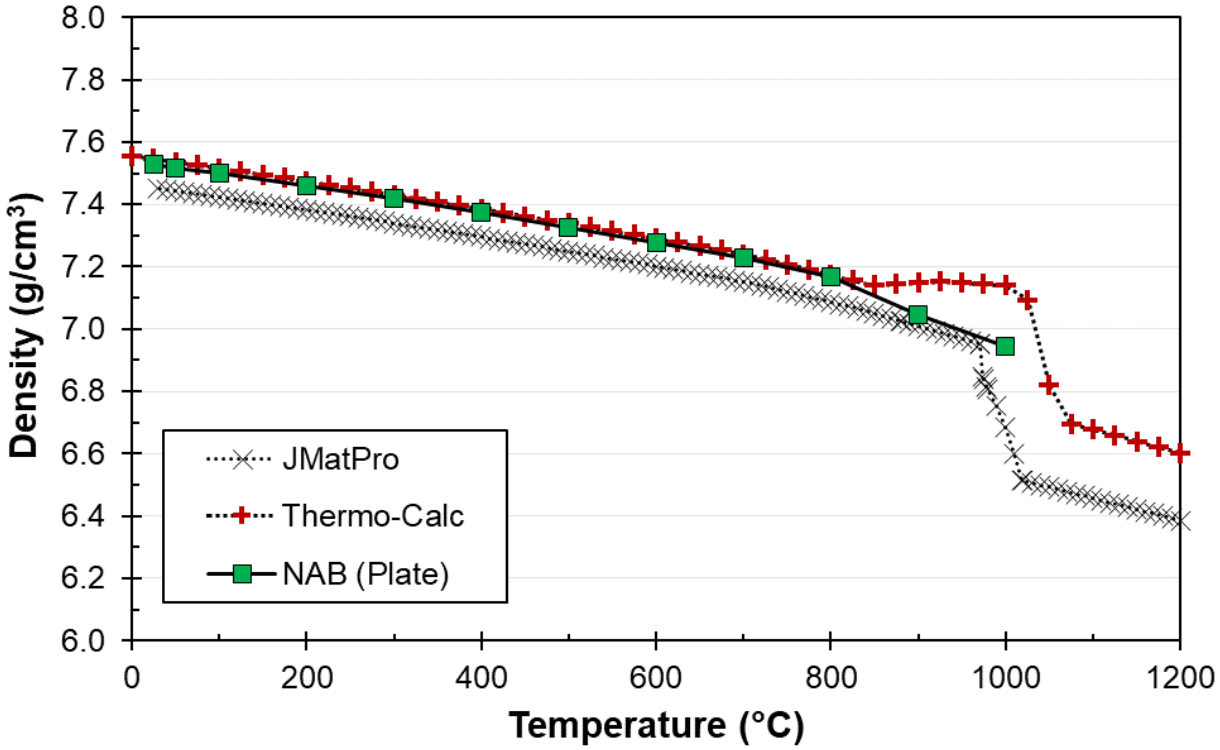

Figure 5. Calculated temperature-dependent density of the NAB plate with *JMatPro* and *Thermo-Calc* predicted values in comparison.

Figure 6-7 shows the temperature-dependent specific heat and thermal diffusivity of the C63200 plate material as measured by TPRL. A comparison to predicted values using *JMatPro* software is included. As shown in **Figure 6,** the measured temperature-dependent specific heat reaches a peak at ~840 °C (1544 °F), which is likely associated with thermal energy absorption from the transformation of α to the β phase [19]. This is fairly consistent with the *JMatPro* prediction, where there is a step at 890 °C (1634 °F), associated with this phase transformation and exhibits a large peak at 970 °C (1778 °F), where the onset of melting is predicted. The *JMatPro* prediction for specific heat is in reasonable agreement with the experimentally measured results, but a significant deviation is exhibited for the predicted thermal diffusivity as shown in **Figure 7**.

The temperature-dependent thermal conductivity shown in **Figure 8** was calculated by multiplying the specific heat, thermal diffusivity, and density at a given temperature (**Equation 3**). A comparison to predicted values using *JMatPro* software is included. As these thermo-physical property values are interrelated, the significant deviation of measured and predicted values for thermal conductivity was not unexpected. Although the experimental and predicted results are relatively consistent for specific heat, the deviation in the thermal diffusivity and density led to differences for the predicted thermal conductivity using *JMatPro*.

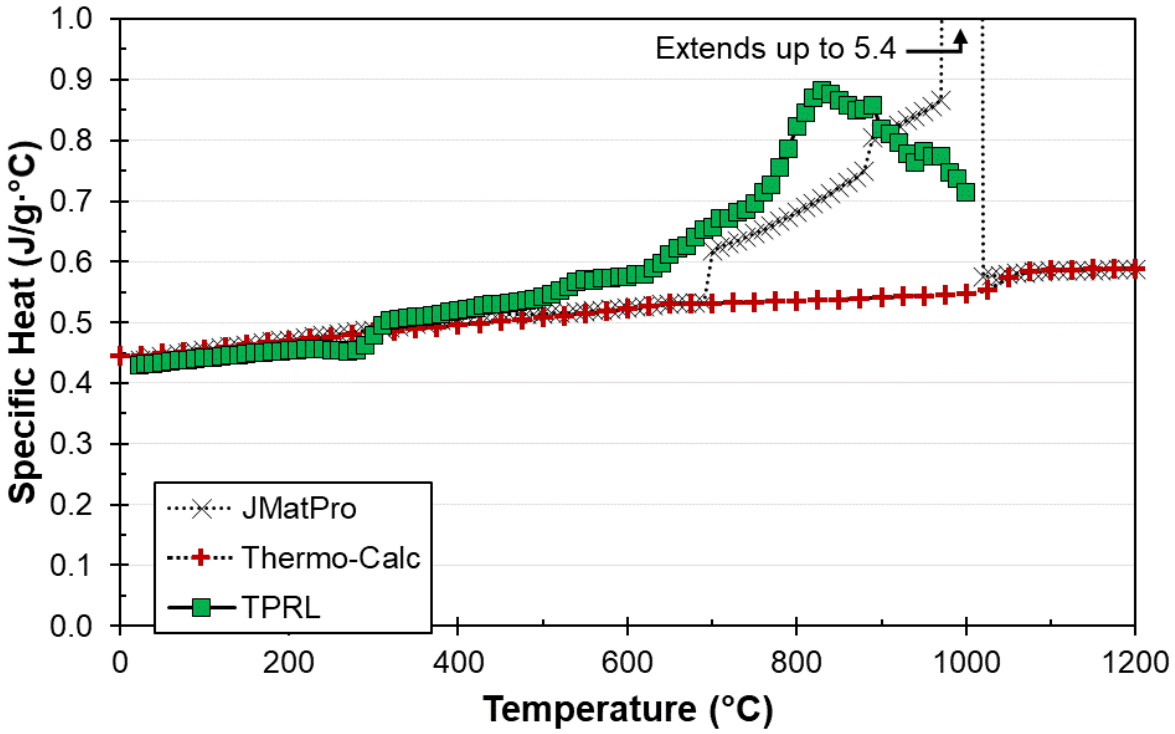

Figure 6. Temperature-dependent specific heat of the NAB plate measured from TPRL with *JMatPro* and *Thermo-Calc* predicted values in comparison. The large, predicted peak in the *JMatPro* data corresponds with the latent heat of melting.

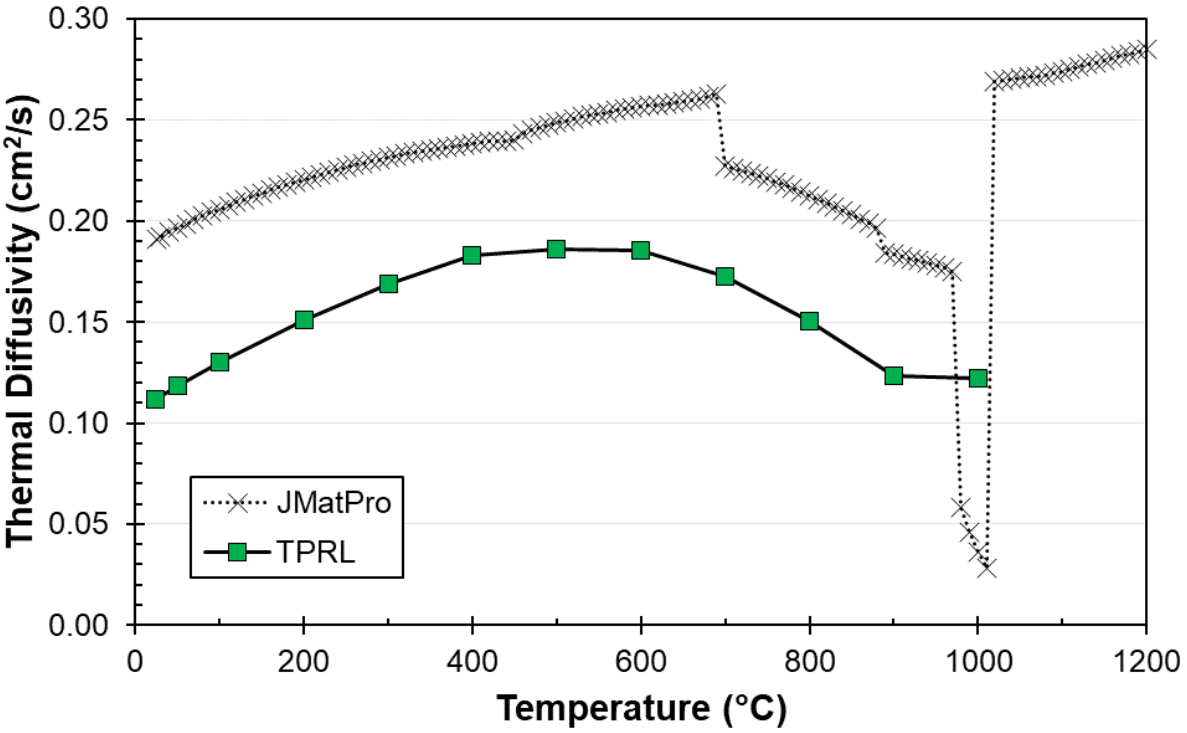

Figure 7. Temperature-dependent thermal diffusivity of the NAB plate measured from TPRL with *JMatPro* predicted values in comparison. The large, predicted valley in the *JMatPro* data corresponds with the latent heat of melting.

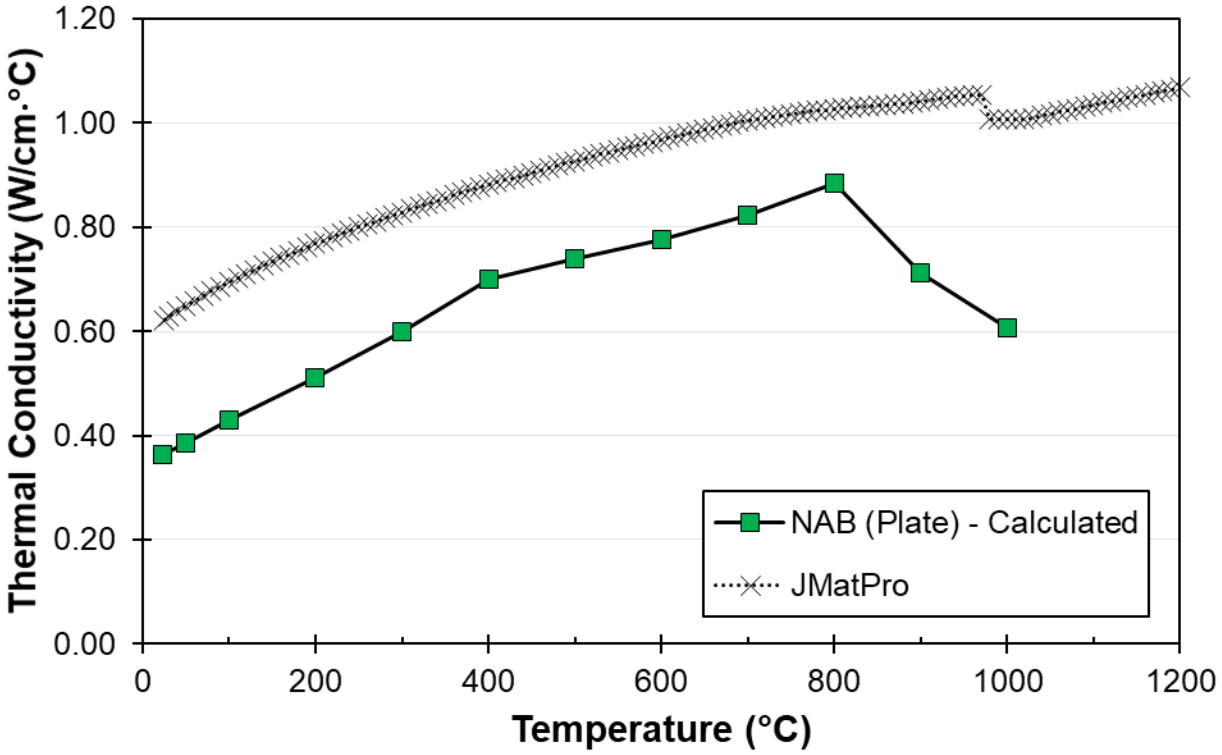

Figure 8. Calculated temperature-dependent thermal conductivity of the NAB plate with *JMatPro* predicted values in comparison.

Thermo-Mechanical Properties

The full stress-strain curves of elevated temperature tensile tests are shown in **Figure 9** for those tested in the Gleeble and **Figure 10** for the samples tested by IMR. An additional test at 900 °C (1652 °F) was completed by IMR, but the load values fell below the calibration settings for IMR's load cell, thus the data are not reported here. It should be noted that there were significant dips in the stress strain curves at elevated temperatures (400 °C [752 °F] and above) that could not be explained by specimen slippage within the grips. Interestingly, the phenomena was not found during the Gleeble testing at NSWCCD (**Figure 11**), but was found in the testing at IMR (**Figure 12**). While this difference is likely caused by the differences in test apparatus, sample size, and test procedure across the two facilities, the observed property is likely a form of yield point phenomena. However, explanation of this elevated temperature yield point phenomena falls outside the scope of this report. Therefore, the reader is encouraged to learn more on the topic starting with reference [20].

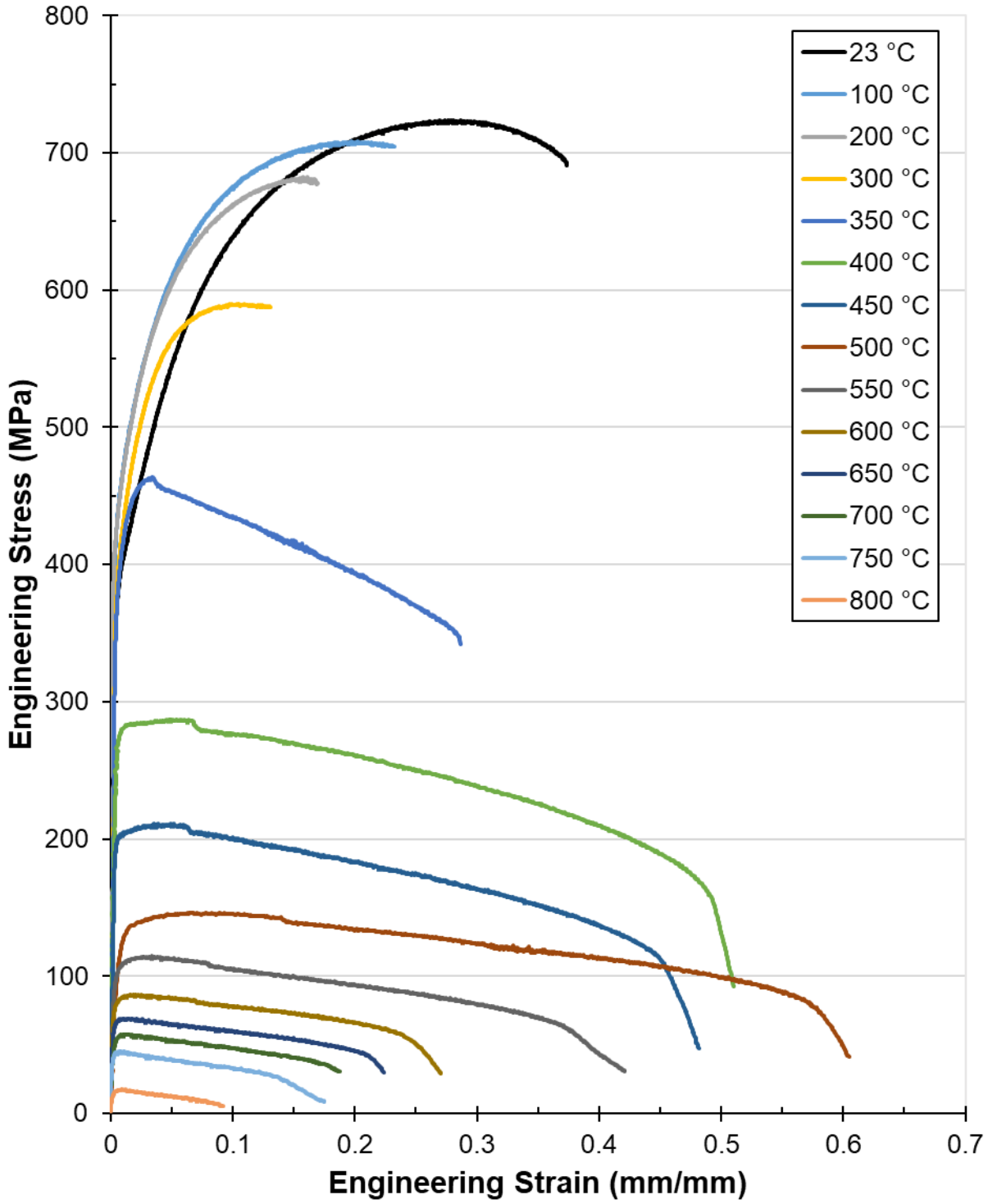

Figure 9. Stress-strain curves of the samples tested in the Gleeble system as a function of temperature.

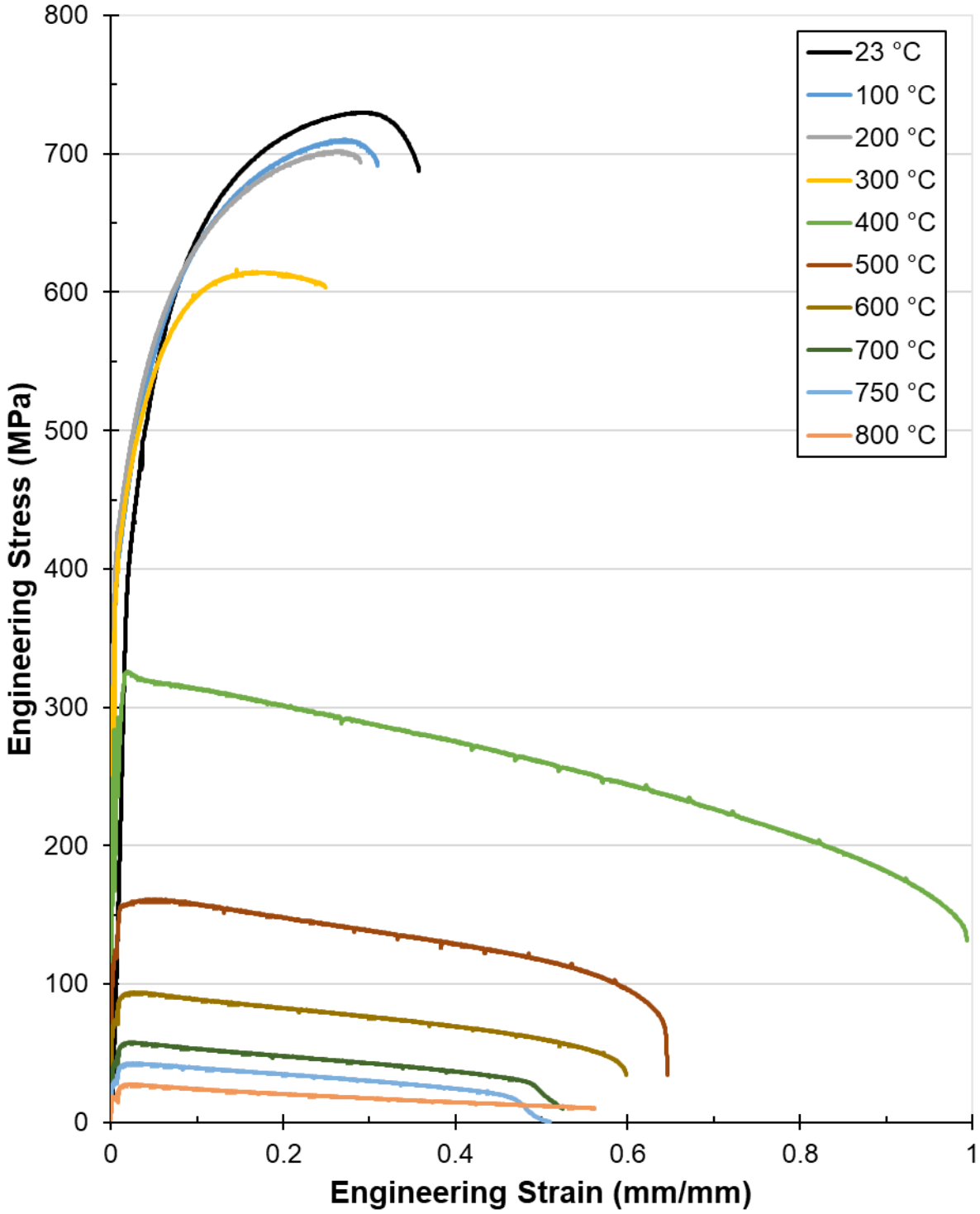

Figure 10. Stress-strain curves of the samples tested by IMR test labs as a function of temperature.

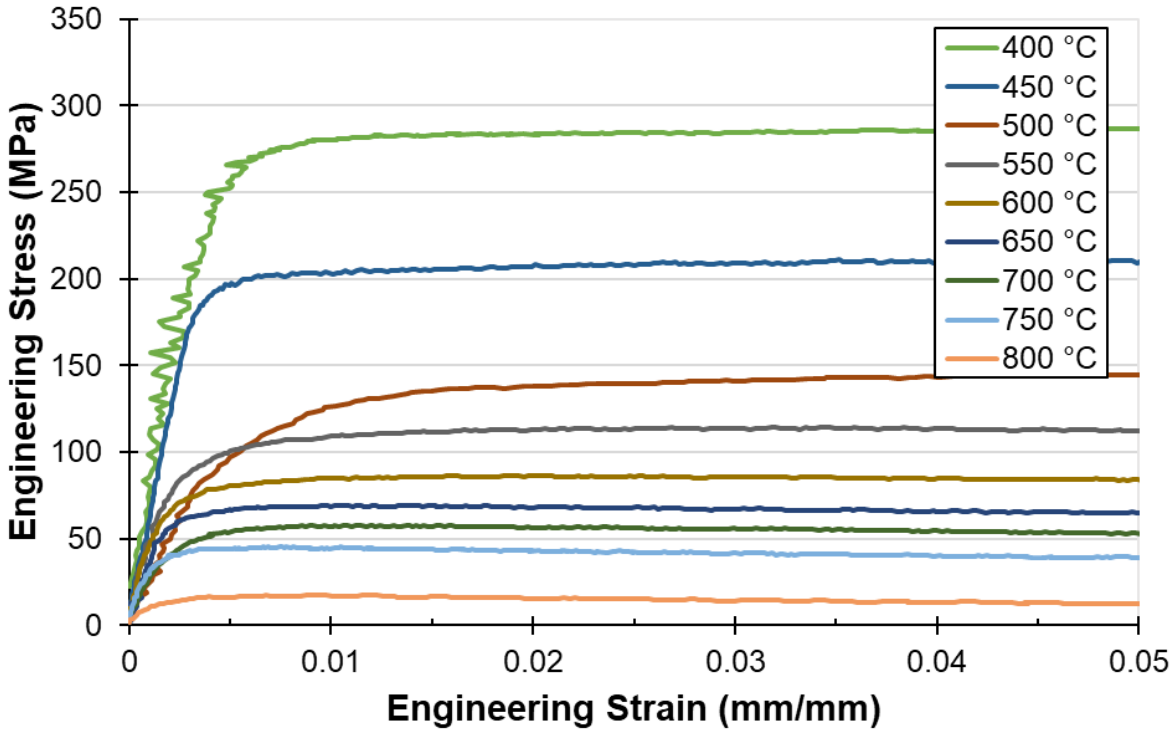

Figure 11. Elevated temperature (tested at 400 °C [752 °F] and above) stress-strain curves of the samples tested in the Gleeble system highlighting the lack of yield point phenomena. Note the strain axis was truncated to 0.05 in order to highlight the effect.

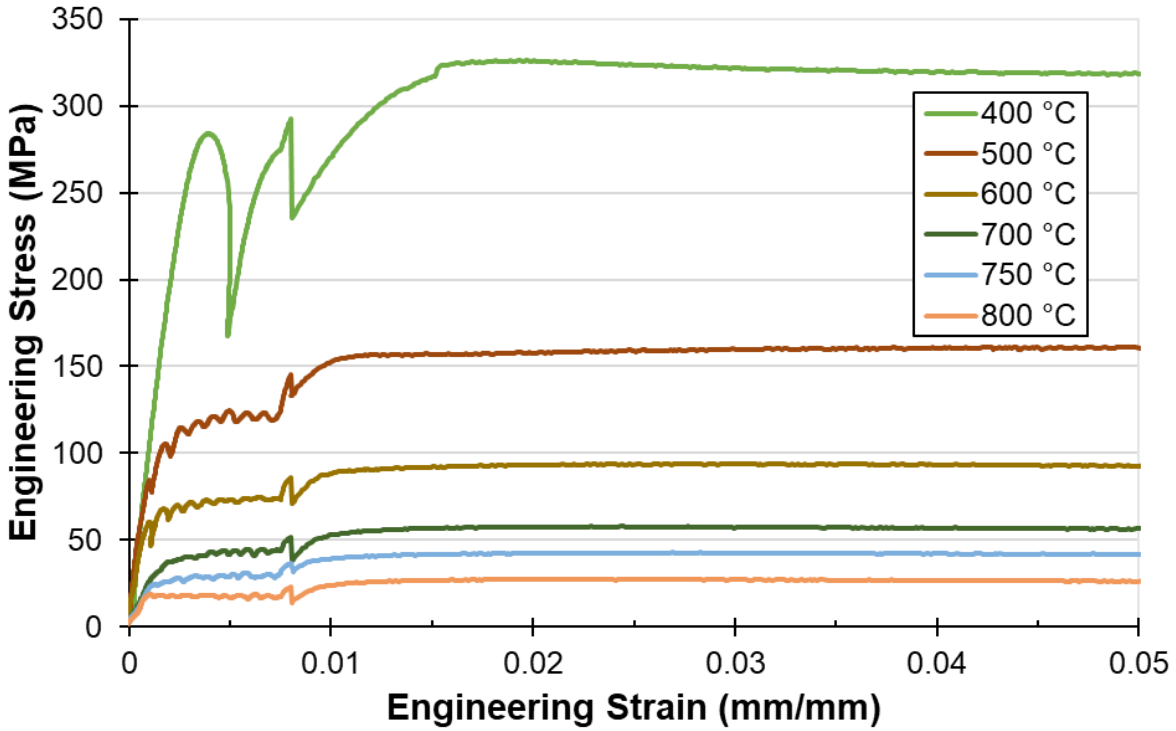

Figure 12. Elevated temperature (tested at 400 °C [752 °F] and above) stress-strain curves of the samples tested by IMR test lab highlighting the possible yield point phenomena. Note the strain axis was truncated to 0.05 in order to highlight the effect.

Due to the differences in test apparatus, sample size, and test procedure noted previously, there are other variations in the observed properties. The most obvious discrepancy between the test cases is the measured elongation as shown in **Figure 13**, which decreases at temperatures greater than 400 °C (752 °F) for the samples tested in the Gleeble but increases for the samples tested by IMR. This may be associated with the difference in specimen geometry, where a round bar specimen may encourage more necking and therefore a higher elongation value. Alternatively, the slower heating rate of the furnace heating of the IMR samples may have led to a more homogeneous microstructure and, when coupled with the higher stroke rate, created a "chewing gum"-type effect at elevated temperatures.

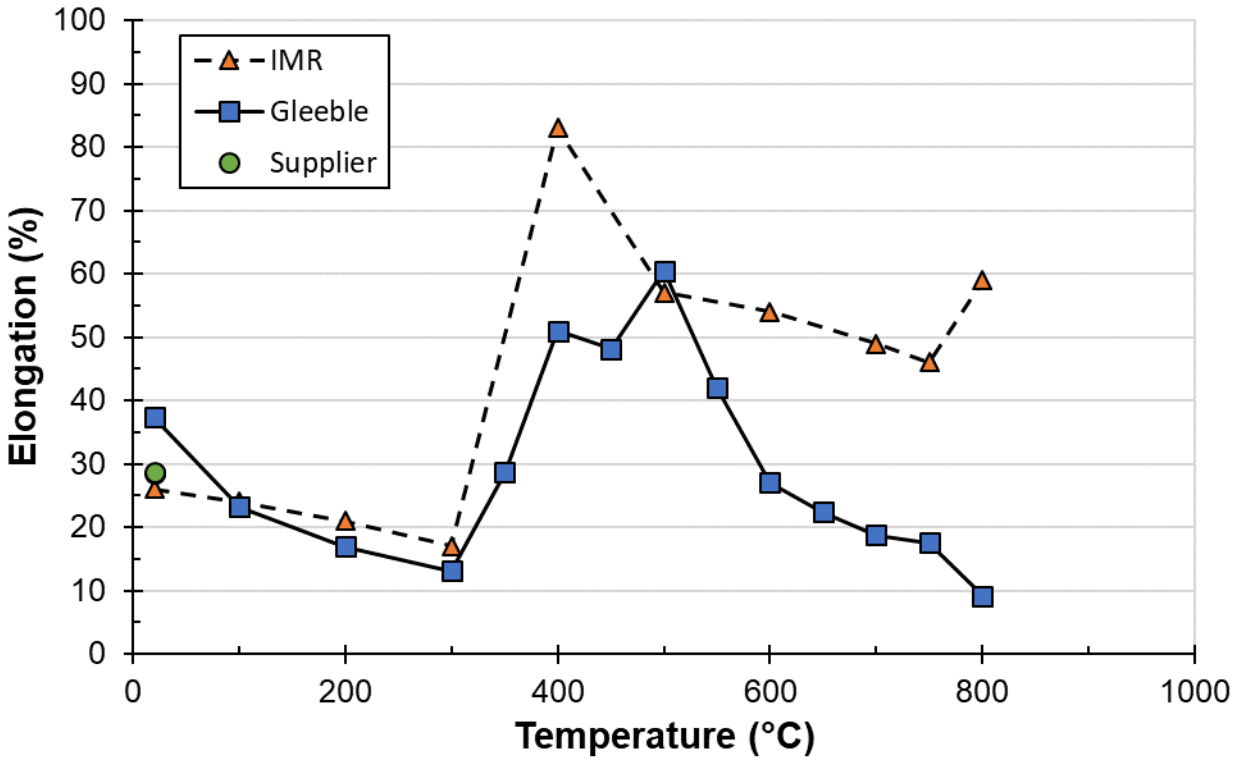

Figure 13. Temperature-dependent elongation of the C63200 plate as measured on the Gleeble and by IMR with two additional room temperature values provided by the material supplier (symbols overlap at this scale).

The linear portion of the stress-strain curves were fit to determine the elastic modulus as shown in **Figure 14.** As stated previously, the elevated temperature mechanical testing was performed in accordance with ASTM E21 [16] for the IMR specimens, whereas the Gleeble specimens did not meet these criteria. However, as the determination of the modulus of elasticity and proportional limit are not covered by ASTM E21 [16] for elevated temperatures (*i.e.*, above room temperature), therefore these elastic moduli are likely inaccurate. This issue with elastic modulus issue could also lead to errors in the determination of the 0.5% offset yield strength. The description of elevated temperature measurement of the elastic modulus is described by ASTM E111 [21], but this does not apply to the Gleeble samples where there is a significant thermal gradient across the gauge length. In both cases, the elastic modulus doesn't begin to decrease until ~200 °C (392 °F), after which there is decrease with increasing temperature. The experimental values are compared to those predicted by *JMatPro*, where there is a more gradual decrease in elastic modulus as a function of temperature and an over-prediction of the elastic modulus at high temperature. In the author's opinion, the copper thermodynamic database for *JMatPro* at the time of writing this report is not as robust as the steel, aluminum, or nickel databases. Namely, it does not allow for the prediction of other mechanical properties, which is why is it absent in the following figures.

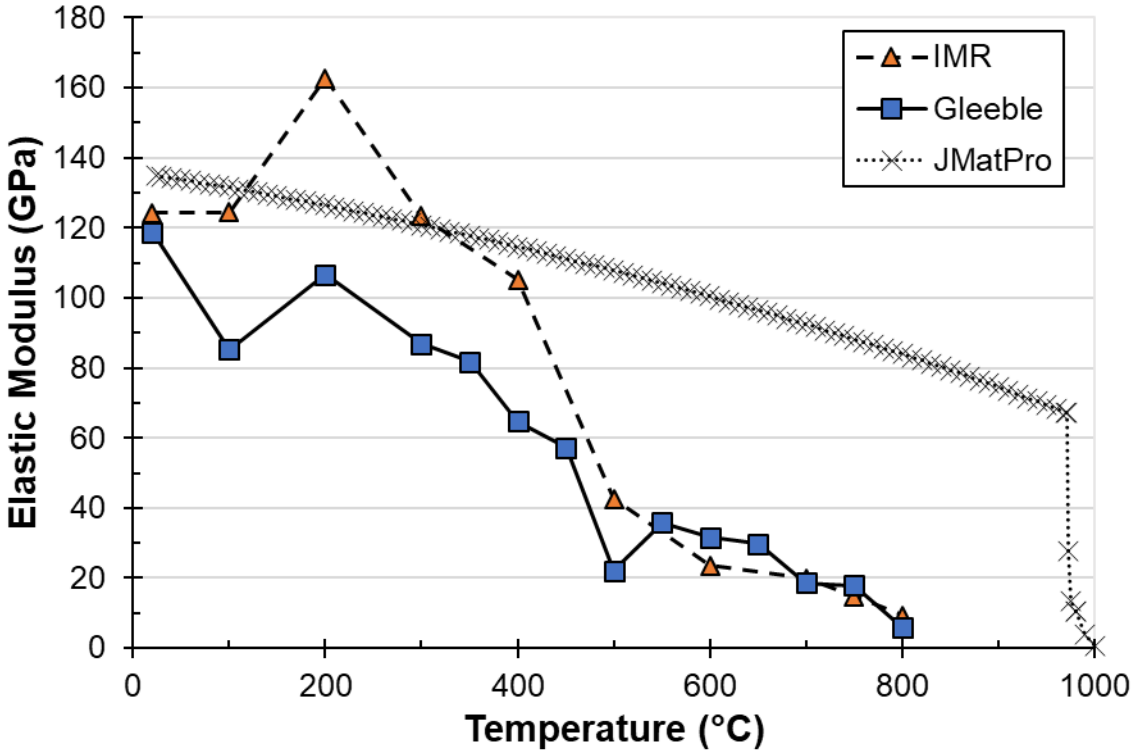

Figure 14. Temperature-dependent elastic modulus of the C63200 plate as measured on the Gleeble and by IMR in comparison to *JMatPro* predicted values.

The experimental trend observed for the elastic modulus is shown more clearly by the temperature-dependent yield strength and UTS, as shown in **Figure 15** and **Figure 16**, respectively. The 0.5% yield strength is more commonly used for NAB materials due to the challenge in separating out the elastic-plastic region with a difference in yield strength of ~5% over the entire temperature range. Both the Gleeble specimens and those tested by IMR are consistent with the results reported by the plate manufacturer at room temperature and exhibit similar trends with a non-linear decrease in strength with increasing temperature after around 300 °C (572 °F). This is likely due to grain recrystallization and precipitate dissolution at higher temperatures. However, after ~500 °C (932 °F), there is a relatively linear decrease in strength, associated with the complete dissolution of the κ strengthening precipitates and grain growth [18][19].

The flow stress curves of the tensile tests conducted in the Gleeble are shown in **Figure 17** and by IMR in **Figure 18**. These curves were obtained by removing the data before the 0.5% offset yield point and zeroing the strain. The trends follow the results discussed previously, with a decrease in strength with increasing temperature and a significant increase in the measured ductility of the IMR samples at higher temperatures.

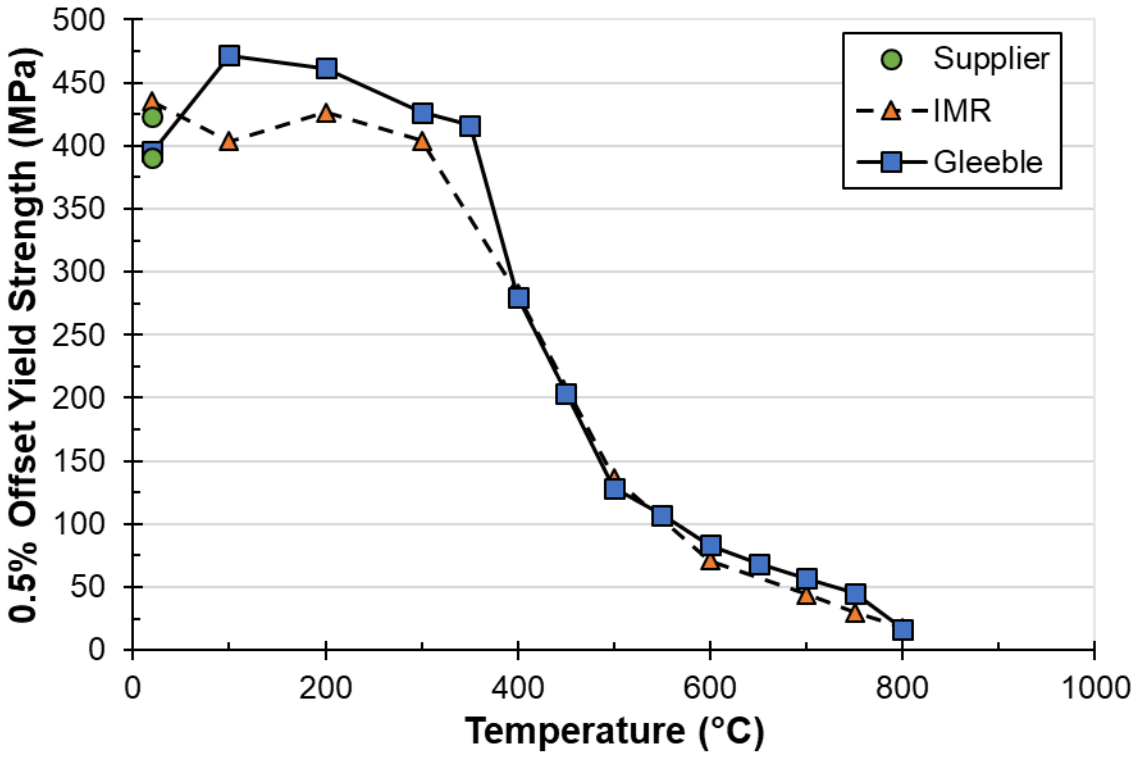

Figure 15. Temperature-dependent 0.5% offset yield strength of the C63200 plate as measured on the Gleeble and by IMR with two additional room temperature values provided by the material supplier.

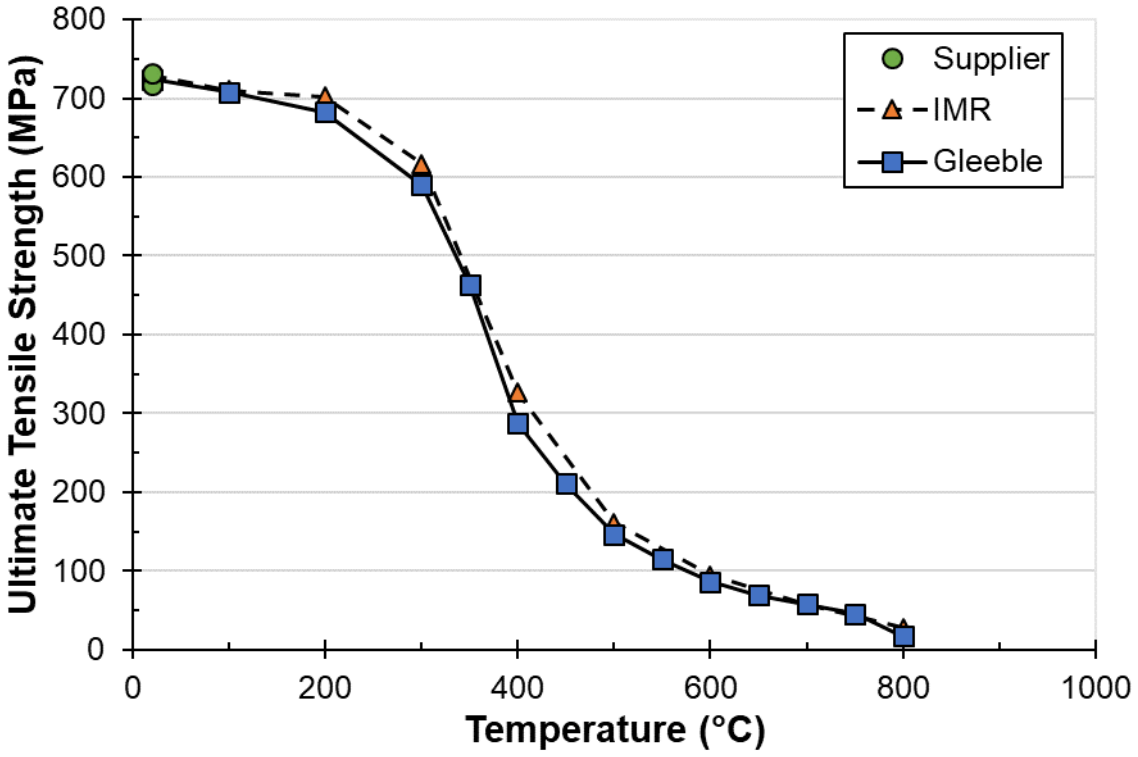

Figure 16. Temperature-dependent UTS of the C63200 plate as measured on the Gleeble and by IMR with two additional room temperature values provided by the material supplier.

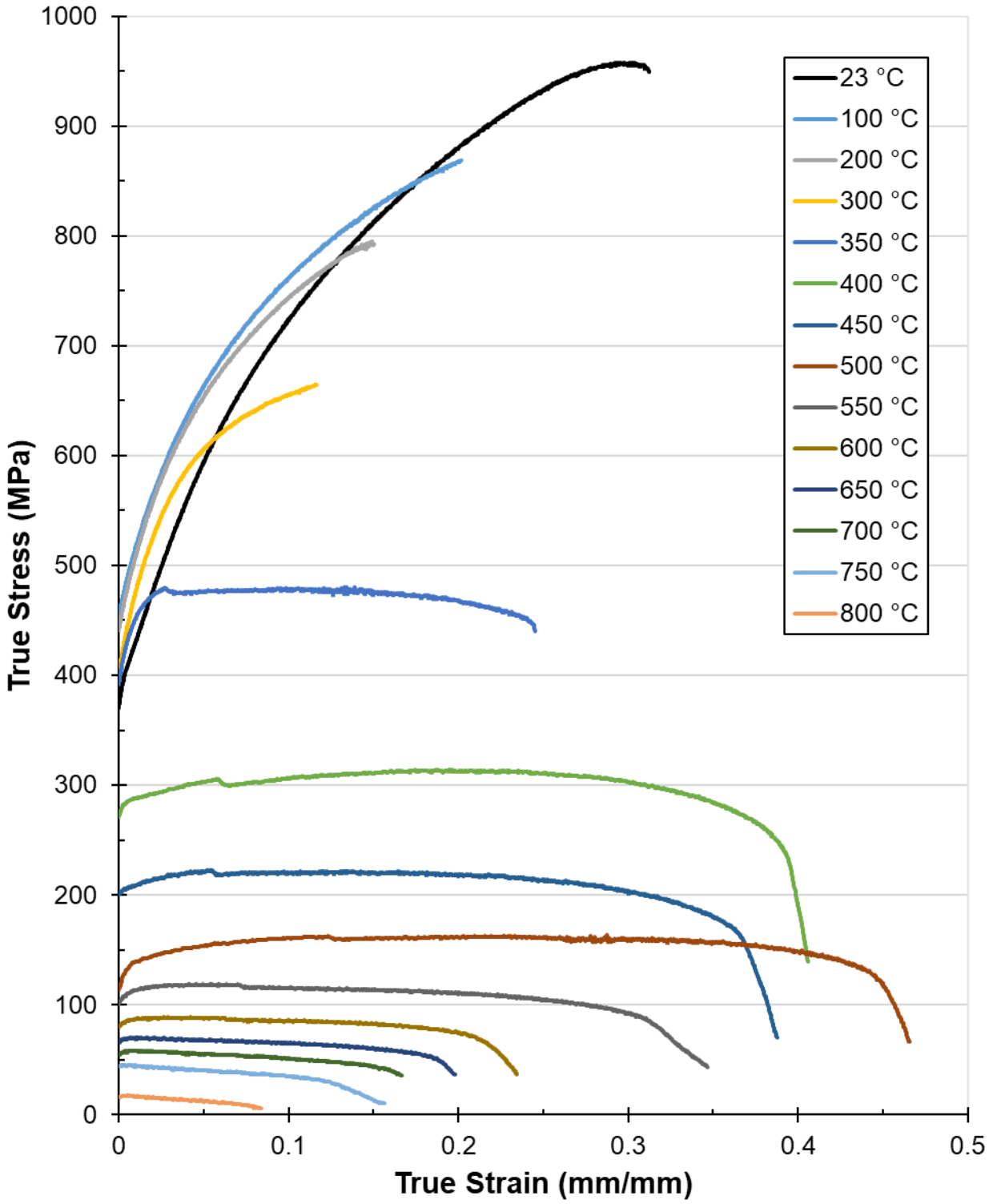

Figure 17. Temperature-dependent flow stress behavior of 63200 plate tested in the Gleeble.

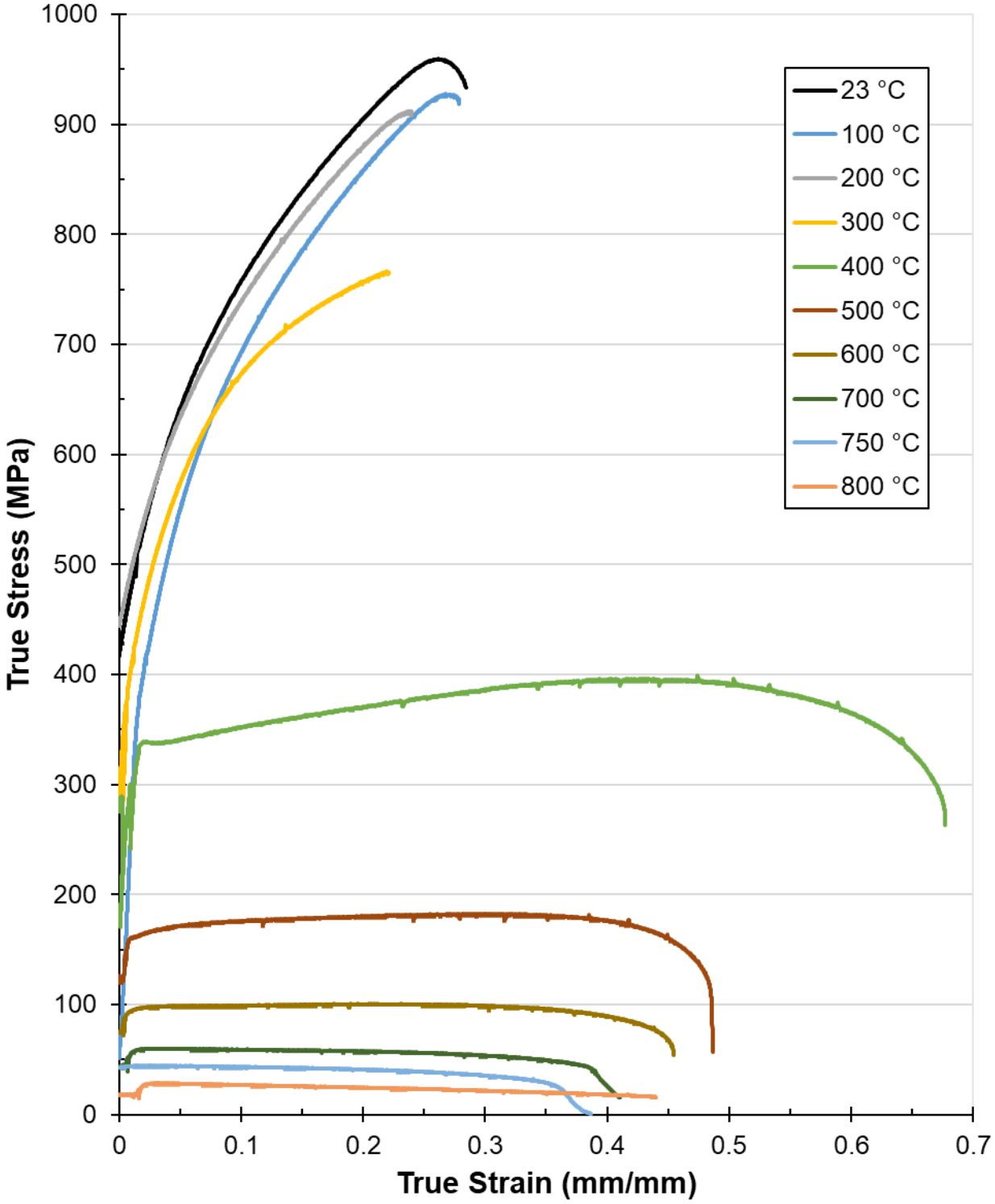

Figure 18. Temperature-dependent flow stress behavior of 63200 plate tested by IMR.

Microstructural Characterization

Figure 19a-b shows an SEM micrograph of the C63200 NAB plate specimen in the as-received condition. The α grains are oriented along the rolling direction and are populated by very fine κ_{IV} (Fe_3Al)

precipitates. These α grains are separated by regions densely populated with κ phases including the globular κ_{II} (Fe_3Al) and lamellar κ_{III} (NiAl). As expected, no martensitic β' phases were observed.

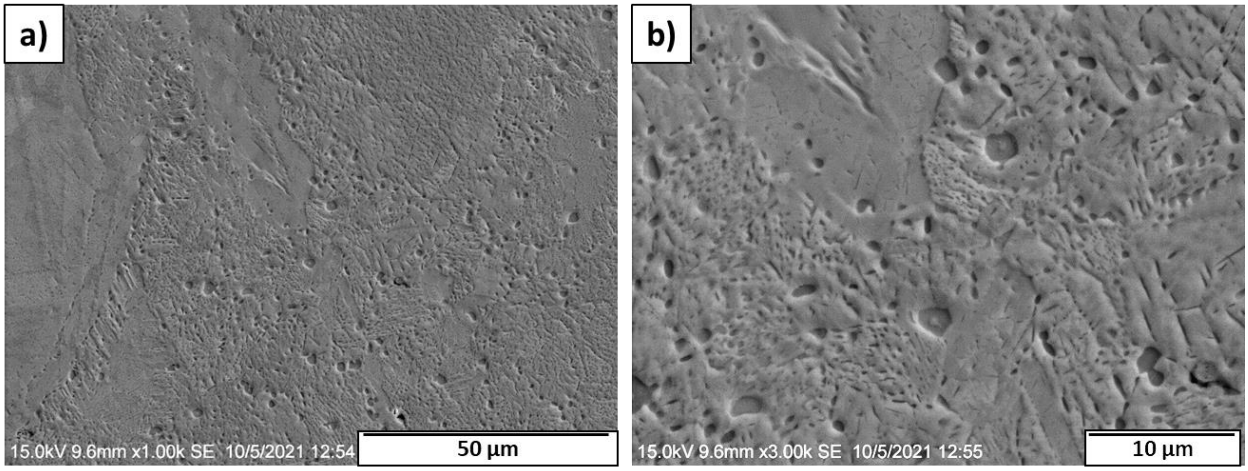

Figure 19. SEM micrograph of the C63200 Plate specimen with **a)** 1000x and **b)** 3000x magnification.

Figure 20a-f shows SEM images of the fracture surface after tensile testing at various temperatures. The dominant fracture mechanism is microvoid coalescence (MVC) for each sample tested below 600 °C (1112 °F) associated with a ductile fracture mode. However, the sample tested at 800 °C (1472 °F) exhibits a brittle, dendritic fracture surface as this is likely in the two-phase $\alpha+\beta$ region with the strengthening κ phases dissolved. This may also be associated with the formation of oxide scale on the fracture surface due to the high temperature exposure.

The microstructures of cross-sectioned tensile specimens are shown in **Figure 21a-f**, where the high temperature exposure did not result in significant microstructural changes until after 600 °C (1112 °F). As shown in **Figure 21e**, the κ_{IV} phases within the α grains decrease in size and are not observable for the sample tested at 800 °C (1472 °F) as shown in **Figure 21f**. However, as the time to failure varied between specimens and the formation/dissolution of phases is time and temperature dependent, the microstructures cannot be directly compared. Previous studies such as one reported by Anantapong *et al.* [22] and previous literature reviews document the microstructural evolution in a more controlled manner [5][6][18].

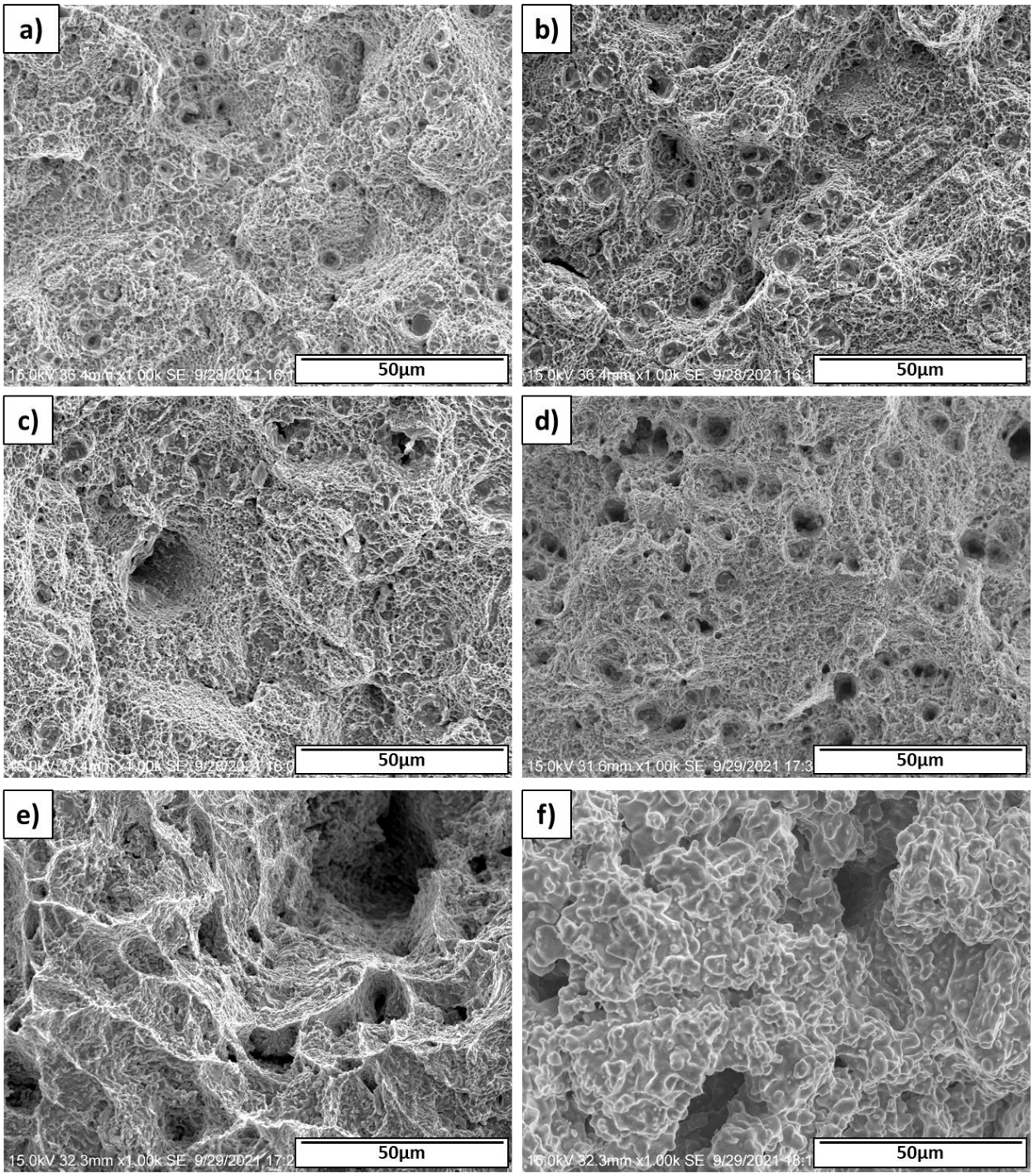

Figure 20. SEM fractography of the specimens tested in the Gleeble at **a)** 20 °C (68 °F); **b)** 200 °C (392 °F); **c)** 300 °C (572 °F); **d)** 400 °C (752 °F); **e)** 600 °C (1112 °F); and **f)** 800 °C (1472 °F).

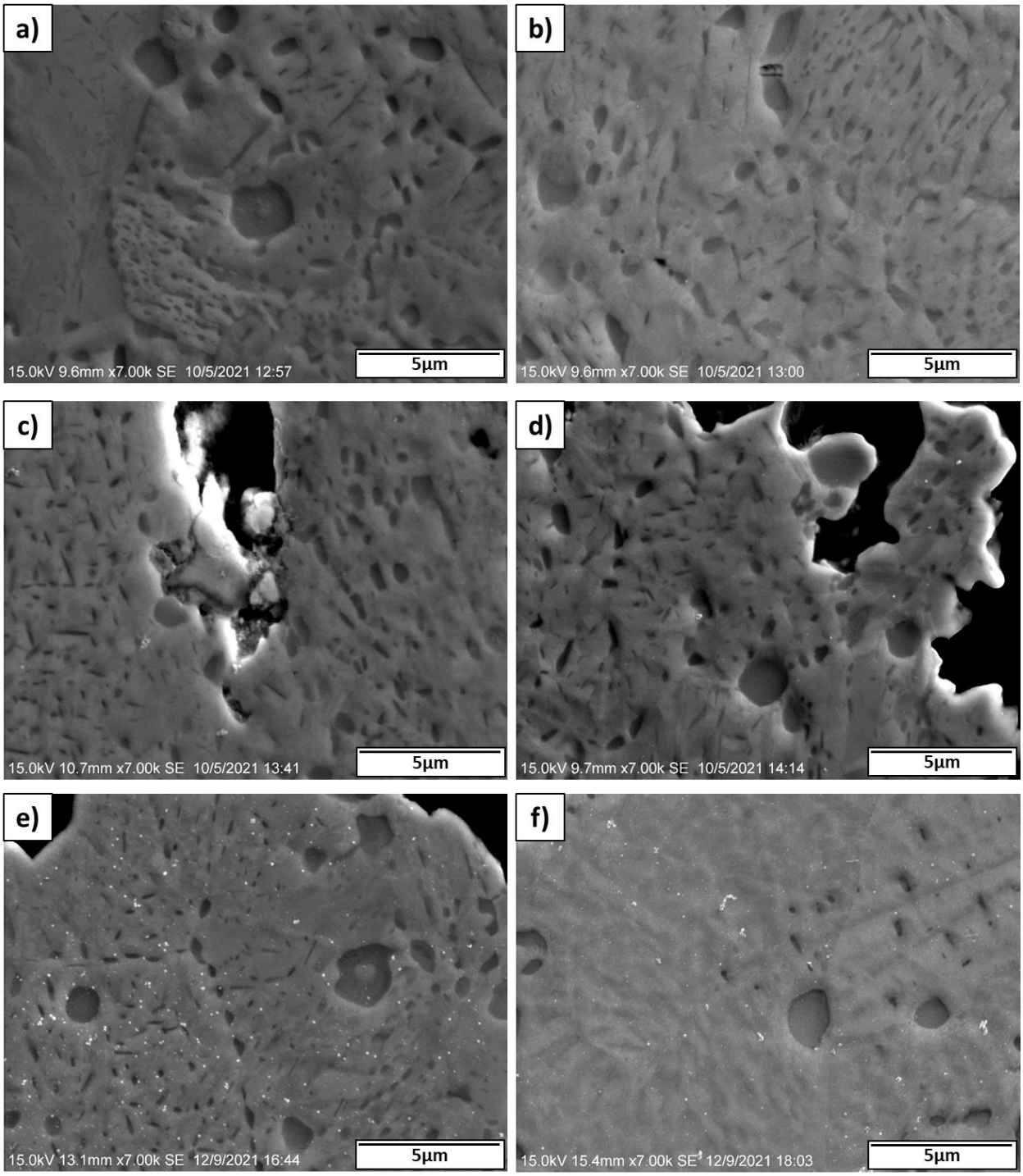

Figure 21. SEM microstructures of the specimens tested in the Gleeble at **a)** 20 °C (68 °F); **b)** 200 °C (392 °F); **c)** 300 °C (572 °F); **d)** 400 °C (752 °F); **e)** 600 °C (1112 °F); and **f)** 800 °C (1472 °F).

SUMMARY

Temperature-dependent material property data of a 63200 NAB plate material from room temperature up to near melting were determined. The thermo-physical properties investigated include specific heat, thermal diffusivity, thermal conductivity, CTE, and density. The experimentally measured results correspond well with the *JMatPro* predicted values for CTE as well as the predicted specific heat for both *JMatPro* and *Thermo-Calc*, particularly at 400 °C (752 °F) and below. The predicted density values from both software tools were also noted to be fairly aligned with the measured data. However, the *JMatPro* software was unable to determine accurate values for thermal diffusivity and thermal conductivity (which are admittedly inter-related) nor for the liquidus and solidus temperatures. *Thermo-Calc* is not currently able to predict any of those values directly. The authors hope to achieve higher accuracy with future iterations of the Cu database in future updates from Sente as well as additional models integrated in the *Thermo-Calc* software using their Cu database to enable users to predict more properties.

Thermo-mechanical properties including elastic modulus, yield strength, UTS, elongation, and flow stress were also measured. At the time of writing, mechanical properties (outside of elastic modulus) cannot be predicted using *JMatPro* for copper alloys and therefore are not included for discussion. The tensile strength of the NAB alloy does not significantly change at temperatures below 200 °C (392 °F). Between ~250 and 500 °C (~482-932 °F), there is a significant reduction in tensile properties. A more gradual reduction in strength occurred at temperatures exceeding 550 °C (1022 °F). Due to the lack of volumetric change associated with the microstructural transformations in NAB, a CCT diagram could not be developed using currently available equipment.

This material testing effort is essential for increasing the fidelity of finite element models used to predict welding and large-scale AM fabrication-induced distortion and residual stress in marine structures. The data generated in this program have been provided to ESI for incorporation into their *SYSWELD* software and to Hexagon for incorporation into their *Simufact Welding* software. A machine-readable version of the collected data has been uploaded to the University of Michigan's *Materials Commons* data repository: https://materialscommons.org/ [23].

REFERENCES

[1] I. Richardson, “Guide to Nickel Aluminium Bronze for Engineers,” ed. C. Powell, Copper Development Association, Publication No. 222, January 2016. https://copper.org/applications/marine/nickel_al_bronze/pub-222-nickel-al-bronze-guide-engineers.pdf

[2] *ASM Specialty Handbook: Copper and Copper Alloys*, ed. J. R. Davis, ASM International, 2001.

[3] J. A. Wharton, R. C. Barik, G. Kear, R. J. K. Wood, K. R. Stokes, and F. C. Walsh, “The Corrosion of Nickel-Aluminium Bronze in Seawater,” *Corrosion Science*, vol. 47, no. 12, pp. 3336–3367, December 2005. DOI: 10.1016/j.corsci.2005.05.053

[4] G. M. Weston, “Survey of Nickel-Aluminium-Bronze Casting Alloys on Marine Applications,” MRL-R-807, Defence Science and Technology Organisation – Materials Research Laboratory, Melbourne, Victoria, Australia, 1981.

[5] P. Brezina, “Heat Treatment of Complex Aluminium Bronzes,” *International Metals Reviews*, vol. 27, no. 1, pp. 77–120, 1982.

[6] S. M. Orzolek, J. K. Semple, and C. R. Fisher, “Nickel-Aluminum Bronze (NAB) Review: Additive Manufacturing and Weldability,” NSWCCD-61-TR-2021/9, June 2021. https://apps.dtic.mil/sti/pdfs/AD1147115.pdf

[7] M. Seifi, A. Salem, J. Beuth, O. Harrysson, and J. J. Lewandowski, “Overview of Materials Qualification Needs for Metal Additive Manufacturing,” *JOM*, vol. 68, pp. 747-764, January 2016. DOI: 10.1007/s11837-015-1810-0

[8] J. K. Semple, D. H. Bechetti, W. Zhang, and C. R. Fisher, “Temperature-Dependent Material Property Database for Marine Steels – Part 3: HSLA-80,” NSWCCD-61-TR-2020/24, October 2020. https://apps.dtic.mil/sti/pdfs/AD1173997.pdf

[9] J. K. Semple, D. H. Bechetti, W. Zhang, and C. R. Fisher, “Temperature-Dependent Material Property Database for Marine Steels – Part 2: HSLA-65,” NSWCCD-61-TR-2020/03, June 2020. https://apps.dtic.mil/sti/pdfs/AD1121145.pdf

[10] D. H. Bechetti, J. K. Semple, W. Zhang, and C. R. Fisher, “Temperature-Dependent Material Property Databases for Marine Steels—Part 1: DH36,” NSWCCD-61-TR-2019/03, May 2019. https://apps.dtic.mil/sti/pdfs/AD1137608.pdf

[11] ASTM B150/B150M-19, “Standard Specification for Aluminum Bronze Rod, Bar, and Shapes,” ASTM International, West Conshohocken, PA, 2019. DOI: 10.1520/B0150_B0150M-19

[12] ASTM E415-21, "Standard Test Method for Analysis of Carbon and Low-Alloy Steel by Spark Atomic Emission Spectrometry," ASTM International, West Conshohocken, PA, 2017. DOI: 10.1520/E0415-21

[13] ASTM E1461-13, "Standard Test Method for Thermal Diffusivity by the Flash Method," ASTM International, West Conshohocken, PA, 2013. DOI: 10.1520/E1461-13R22

[14] ASTM E1269-11, "Standard Test Method for Determining Specific Heat Capacity by Differential Scanning Calorimetry," ASTM International, West Conshohocken, PA, 2018. DOI: 10.1520/E1269-11R18

[15] ASTM A370-21, "Standard Test Methods and Definitions for Mechanical Testing of Steel Products," ASTM International, West Conshohocken, PA, 2018. DOI: 10.1520/A0370-21

[16] ASTM E21-20, "Standard Test Methods for Elevated Temperature Tension Tests of Metallic Materials," ASTM International, West Conshohocken, PA, 2020. DOI: 10.1520/E0021-20.

[17] ASTM E8/E8M-21, “Standard Test Methods for Tension Testing of Metallic Materials,” ASTM

International, West Conshohocken, PA, 2021. DOI: 10.1520/E0008_E0008M-21.

[18] C. V. Hyatt, “Review of Literature Related to Microstructure Development during Laser Surface Engineering of Nickel Aluminium Bronze,” Defence Research Establishment Atlantic, Technical Memorandum 96/227, March 1997.

[19] F. Hasan, A. Jahanafrooz, G. W. Lorimer, and N. Ridley, “The morphology, crystallography, and chemistry of phases in as-cast nickel-aluminum bronze,” *Metallurgical Transactions A*, vol. 13, no. 8, pp. 1337–1345, 1982. DOI: 10.1007/BF02642870.

[20] R. Schwab and V. Ruff, “On the nature of the yield point phenomenon,” *Acta Materialia*, vol. 61, no. 5, pp. 1798-1808, 2013. DOI: 10.1016/j.actamat.2012.12.003.

[21] ASTM E111-17, "Standard Test Method for Young's Modulus, Tangent Modulus, and Chord Modulus," ASTM International, West Conshohocken, PA, 2017. DOI: 10.1520/E0111-17.

[22] J. Anantapong, V. Uthaisangsuk, S. Suranuntchai, and A. Manonukul, “Effect of hot working on microstructure evolution of as-cast Nickel Aluminum Bronze alloy,” *Materials and Design*, vol. 60, pp. 233–243, August 2014. DOI: 10.1016/j.matdes.2014.03.033.

[23] S. Orzolek, J.E. Norkett, and C.R. Fisher, "Temperature-Dependent Material Property Database: NAB (Plate)," 20 September 2023. [Online]. Available: https://doi.org/10.13011/m3-tzyf-xc43.

APPENDIX A: NAB Plate Data Sheet

Where Quality Isn't Expensive.....It's Priceless!

DIVERSIFIED METALS
INCORPORATED

TOLL FREE: 800-628-3035
EMAIL: SALES@DIVERSIFIEDMETALS.COM
WEBSITE: WWW.DIVERSIFIEDMETALS.NET
49 MAIN STREET MONSON, MA 01057-0065

FAX: 413-267-3151
PHONE: 413-267-5101
CAGE CODE: 57067
PO BOX 65

MATERIAL CERTIFICATION

Customer:
NAVAL SURFACE WARFARE CENTER
9500 MACARTHUR BLVD
BLDG143
BETHESDA, MD 20817

Ship To Address:
NAVAL SURFACE WARFARE CENTER
9500 MACARTHUR BLVD
BLDG143
BETHESDA, MD 20817

Customer Order: 4521631751

Item No.: 1

P/N: NONE

Dimensions: 1.00" THK X 8.00" WD X 12.250" EA

Alloy/Grade: ALUMINUM BRONZE C63200 TQ50

SPECIFICATION: ASTM-B150(12-17)

No. of Skids	*No. of Pieces*	*Total Quantity Shipped*	*Weight Shipped*	*Packing Slip No.*	*Heat No.*	*Lot No.*
1	20	12.250" EA PC	590.0 LBS	122273	H3014	L38206

MILL TEST REPORT ATTACHED

MATERIAL WAS NOT EXPOSED TO MERCURY WHILE AT DIVERSIFIED METALS' FACILITY.

MATERIAL WAS NOT WELD REPAIRED WHILE AT DIVERSIFIED METALS' FACILITY.

This is to certify that each lot has been sampled, tested and inspected in accordance with the specification and meets all specification requirements.

We certify that the Chemical Analysis and Physical Test Results applying on the above order number are correct and true.

QUALITY APPROVAL:

Lori St George
Lori St George
Quality Control Administrator
quality@diversifiedmetals.com
Date: July 22, 2019

Mill Cert. – REV 3. – 5-3-13

ISO 9001 2015
AS 9100 Rev. D

LEBRONZE ALLOYS UK LTD

TEST CERTIFICATE

EN 10204:2004 3.1

lebronze alloys | UK bolton

CUSTOMER

DIVERSIFIED METALS,INC
49 MAIN STREET

MONSON
MA01057
UNITED STATES

TEST CERTIFICATE No	L38206 Rev : 0
SERIAL / BATCH / LOT No	L38206
CUSTOMER ORDER No	68958
WORKS ORDER No	S43687

SPECIFICATIONS

ASTM B150 (03)(08)(12)(12-17) C63200 TQ50
QQ-C-465B AMD 1 C63200
MIL-B-24059 (3)

DESCRIPTION

CA23 8IN x 1IN Rectangle 72IN Forging (FO)
Nickel Aluminium Bronze

WEIGHT ORDERED (Kg)	503
WEIGHT DESPATCHED (Kg)	575

MECHANICAL / PHYSICAL PROPERTIES

Tensile Specification	Heat No	Dia d	Area So	0.5% Yield Strength E.U.L	U.T.S. Rm	Elongation 4D
ASTM EB 16a		mm	mm2	Ksi	Ksi	%
	H3014	12.49	122.52	56.6	104.1	28.6
		12.48	122.33	61.4	106.2	28.8
	Min			50.0	100.0	18
	Max			n/a	n/a	n/a

CHEMICAL COMPOSITION

Heat No	Zn	Fe	Mn	Al	Sn	Pb	Si	Cu+Ag	Ni+Co	Weight (Kg)
H3014	0.02	3.81	1.35	9.25	0.01	<0.01	0.03	81.00	4.49	575
Min	-	3.50	1.20	9.00	-	-	-	78.00	4.00	
Max	0.30	4.00	1.50	9.50	0.20	0.02	0.10	100.00	4.80	

REMARKS

Residual stress test satisfactory
Country of Melt and Manufacture is UK
No Weld Repairs
We certify that this material was not exposed to Radium or other Radioactive Materials while at our facility.
Heat treated for 1 hr @ 850oc O/Q = 1562oF
Tempered for 3 hrs @ 700oc A.C. = 1292oF
Each lot has been sampled, tested and inspected in accordance with this specification and has met the requirements.
Reported results represent the actual Attributes of the material furnished and are in full compliance with all applicable specification and contract requirements.

Converted by
T M Bagorio
DMI QC Administrator
11/13/18

We certify that material is free from mercury contamination

Signed for on behalf of
LEBRONZE ALLOYS UK LTD

Senior Inspector : J.Gaffney
Signed : 11 Sep 2018

Printed : 19 Sep 2018

UT Report No BAUT 01037 REV 0 Refers

APPROVED BY: TB
DATE: 11/13/18
DIVERSIFIED METALS
TERESA BAGORIO
Q.C. ADMINISTRATOR

DIVERSIFIED METALS, INC
49 MAIN STREET, MONSON, MA
P: 413-267-5101 F: 413-267-3151
SOLD TO: NSWC CARDEROCK
PO: 4521631751 ITEM: 1

Lebronze Alloys UK Ltd
New Way, Hadleigh Road, Ipswich, SUFFOLK, IP2 0BD
Tel: 01473 252 127 Fax: n/a
Email: SalesIpswich@Lebronze-Alloys.com
Company Reg. No.: 1650805

lebronze alloys | UK **bolton** metals

Lebronze Alloys UK Limited Ultrasonic Inspection Report (Certificate)

Customer:	Test Site:	Certificate:	Revision:
Diversified Metals Inc	Lebronze Alloys UK Ltd. (Ipswich)	BAUT 01037	0

Items Tested

Documented Identity	Works Order No.	Heat No.(s)	Alloy	Quantity Tested
L38206	S43687	H3014	CA23	10

Description	8.000" x 1.000" Rec x 72" Forging
Material Specification	ASTM B150 03,08,12 C63200 TQ50 QQ-C-465B AMD 1 (83) C63200

Description of Inspection

Test	Acceptance Standard(s)	Procedure
Ultrasonic	T9074_AS_GIB_010/271 Revision 1 T9074_AS_GIB_010/271 T9074_AS_GIB_010/271 – ACN1	(Bolton Metals operating procedure) NDT UT 02 – Issue 4
Area Tested	100%	

Summary of Test Results

8 Bars Tested

Defects Removed JG

H3014: 4 Whole bars: No flaws indicated, all acceptable to specification.

1 bar: 11" – Centre defects indicated, unacceptable to specification.
64" – No flaws indicated, acceptable to specification

1 bar: 12½" – Centre defects indicated, unacceptable to specification.
61" – No flaws indicated, acceptable to specification.

1 bar: 13½" – Centre defects indicated, unacceptable to specification.
59" – No flaws indicated, acceptable to specification

1 bar: 9" – Centre defects indicated, unacceptable to specification.
28" – No flaws indicated, acceptable to specification.
3" – Centre defect indicated, unacceptable to specification.
35" – No flaws indicated, acceptable to specification.

(Total length of good bar: 527")

Statement of Conformity

All equipment checks have been carried out and verified as per Bolton Aerospace operating procedure: NDT 02 – Issue 3 (Procedure for all Ultrasonic Testing Equipment Checks and Calibration)
Upon review of T9074-AS-GIB 010/271 Revision 1, dated 11th September 2014 and T9074-AS-GIB-010/271 dated 30th April 1997, and ACN-1 dated 16th February 1999, the specifications have been found to be equivalent in all essentials regarding ultrasonic inspection. Material that meets the requirements of the later issue of the specification will be deemed to meet the requirements of the earlier issue.

Test Date	10/09/2018	Signatory	James Turner (James Turner)
Cert. Date	10/09/2018	Qualification	SNT-TC-1A Level 2 Number 11 PCN Level 1 Number 334948 (www.bindt.org/PCN)

Lebronze Alloys UK Ltd
New Way, Hadleigh Road, Ipswich, Suffolk, IP2 0BD, United Kingdom
Tel: +44 (0) 1473 252127
SalesIpswich@Lebronze-Alloys.com

Approved to ISO 9001:2015, AS9100 Rev D. Certification No LRQ0902066
Reg No: 1650805 Vat Reg No: GB 369 8669 71

lebronze alloys | UK bolton metals

Lebronze Alloys UK Limited Ultrasonic Inspection Report (Ultrasonic Test Summary)

Customer:	Certificate:	Revision:
Diversified Metals Inc	BAUT 01037	0

Scan Pattern Diagram

Scan 1: 100%

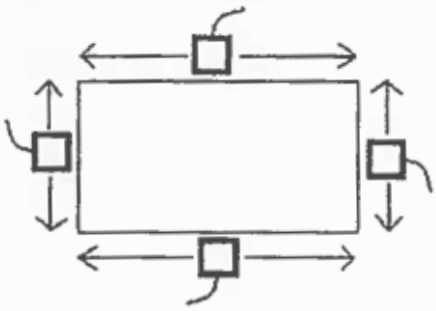

Surface Condition	Smooth	Couplant	Sonatest Sonagel D1
Flaw Detector	Sonatest Masterscan D-70 (S. No. I013467)		
Sketch of Reference Block:		Test Block Material	CA23 (Aluminium Bronze)

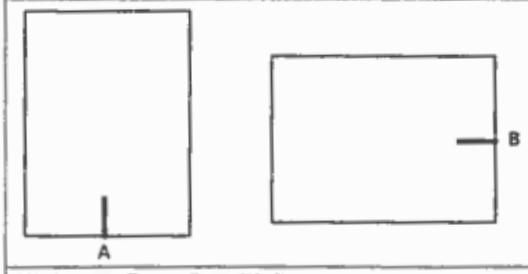

Minimum Scan Sensitivity

Holes Used	Diameter of FBH	Depth of FBH	Signal Amplitude
A	1/4"	1.0"	80%
B	1/16"	1.0"	80%
C			

Zone	Mode of Examination	Probe						Attenuation (dB)	Suppression	Test Block
		Number	Model	Type	Size	MHz	Angle			
Scan 1 (A)	Compression	BA2.25 - 15	CD 2 - 20	Double	17mm x 6mm	2.25	0°	69.5	None	BTB 79
Scan 2 (B)	Compression	BA5 - 44	TC 20 - 5	Double	20mm	5.0	0°	67.5	None	BTB 79

Tested by:	James Turner	Date	10/09/2018

APPENDIX B: Chemical Composition

Table 2. Chemical Composition as Measured by LECO GDS 900

	Weight Percent				
Element	**Test 1**	**Test 2**	**Test 3**	**Test 4**	**Average**
Al	9.08	8.99	9.04	9.02	9.0325
C	0.0185	0.0156	0.0155	0.0169	0.016625
Co	0.0114	0.0109	0.0112	0.0108	0.011075
Cr	0.00147	0.00141	0.00145	0.00143	0.00144
Cu	81.1	81.3	81.2	81.3	81.225
Fe	3.89	3.85	3.84	3.81	3.8475
Mn	1.23	1.22	1.22	1.23	1.225
Nb	0.0135	0.0131	0.0135	0.0129	0.01325
Ni	4.51	4.45	4.5	4.47	4.4825
Pb	0.00371	0.00323	0.00346	0.00345	0.0034625
S	0.00377	0.00382	0.0036	0.00372	0.0037275
Si	0.0329	0.0327	0.0327	0.0343	0.03315
Sn	0.0172	0.0174	0.017	0.0169	0.017125
Ti	0.00394	0.00401	0.00377	0.00388	0.0039
Zn	0.0644	0.0621	0.0621	0.0631	0.062925

APPENDIX C: Thermo-Physical Data

Table 3. DSC Results Summary of Solidification Properties

Liquidus (°C)	Solidus (°C)	Latent Heat of Fusion (J/g)
1086	1061	115.30

Table 4. Measured Coefficient of Thermal Expansion (CTE) Values. Note that CTE was calculated from a linear fit of the 20 – 720 °C on-heating data for the values between 800 and 1000 °C.

Temperature (°C)	Coefficient of Thermal Expansion (mm/mm·°C)
30	1.622E-05
50	1.609E-05
100	1.661E-05
200	1.835E-05
300	1.838E-05
400	2.005E-05
500	2.268E-05
600	2.280E-05
700	2.623E-05
720	2.594E-05
800*	2.667E-05
900*	2.811E-05
1000*	2.955E-05

Table 5. Measured Specific Heat Capacity

Temperature (°C)	Specific Heat (W-s/g-K)	Temperature (°C)	Specific Heat (W-s/g-K)	Temperature (°C)	Specific Heat (W-s/g-K)
23	0.4298	350	0.5088	680	0.6408
30	0.431	360	0.5097	690	0.6531
40	0.4325	370	0.5115	700	0.658
50	0.4341	380	0.5138	710	0.6707
60	0.4356	390	0.5168	720	0.6723
70	0.4371	400	0.5199	730	0.6812
80	0.4386	410	0.5222	740	0.6848
90	0.4401	420	0.5246	750	0.6964
100	0.4417	430	0.5272	760	0.7149
110	0.4428	440	0.5292	770	0.726
120	0.444	450	0.531	780	0.7561
130	0.4453	460	0.5324	790	0.7863
140	0.4469	470	0.5339	800	0.8226
150	0.4479	480	0.5358	810	0.8465
160	0.4495	490	0.5389	820	0.8701
170	0.4511	500	0.5419	830	0.8823
180	0.4517	510	0.5467	840	0.876
190	0.4526	520	0.5522	850	0.8662
200	0.4537	530	0.5581	860	0.8576
210	0.4547	540	0.5662	870	0.8495
220	0.4554	550	0.5704	880	0.8518
230	0.4554	560	0.5693	890	0.8585
240	0.4556	570	0.5737	900	0.8181
250	0.455	580	0.5722	910	0.8111
260	0.4535	590	0.5742	920	0.7964
270	0.4521	600	0.5758	930	0.7772
280	0.4542	610	0.5794	940	0.7641
290	0.4631	620	0.5791	950	0.7814
300	0.4787	630	0.5889	960	0.7742
310	0.4946	640	0.5981	970	0.773
320	0.5032	650	0.6125	980	0.748
330	0.506	660	0.6225	990	0.7367
340	0.5073	670	0.627	1000	0.7143

Table 6. Measured Thermo-Physical Property Summary

Temperature (°C)	Thermal Conductivity (W/cm-K)	Specific Heat (W-s/g-K)	Thermal Diffusivity (cm^2/sec)	Density (g/cm^3)
23	0.3623	0.4298	0.1120	7.527
50	0.3858	0.4341	0.1182	7.518
100	0.4306	0.4417	0.1300	7.499
200	0.5114	0.4537	0.1511	7.459
300	0.5991	0.4787	0.1687	7.419
400	0.7006	0.5199	0.1828	7.374
500	0.7382	0.5419	0.1860	7.325
600	0.7771	0.5758	0.1854	7.278
700	0.8217	0.6580	0.1728	7.227
800	0.8854	0.8226	0.1502	7.166
900	0.7118	0.8181	0.1235	7.046
1000	0.6065	0.7143	0.1223	6.945

APPENDIX D: Thermo-Mechanical Data

Table 7. Tensile Result Summary of High-Temperature Tensile Tests Conducted by IMR and in the Gleeble (SI Units)

Temperature (°C)	Test Provider	UTS (MPa)	0.2% Yield Stress (MPa)	0.5% Yield Stress (MPa)	Elastic Modulus (GPa)	Failure Stress (MPa)	Max Strain (mm/mm)	Average Strain Rate (s^{-1})
20	IMR	730.04	404.24	435.30	124.29	407.95	0.34	1.69E-03
20	Gleeble	723.82	368.51	395.45	118.79	691.12	0.37	4.44E-04
100	IMR	710.27	372.80	403.74	124.38	691.36	0.31	8.43E-04
100	Gleeble	708.13	450.88	471.97	85.30	704.75	0.23	3.26E-04
200	IMR	702.13	387.96	426.70	162.64	401.58	0.29	8.61E-04
200	Gleeble	682.17	438.50	461.30	106.75	677.57	0.17	2.50E-04
300	IMR	616.26	356.68	403.91	123.37	359.43	0.25	8.28E-04
300	Gleeble	589.85	398.74	426.68	86.97	587.55	0.13	3.10E-04
350	Gleeble	463.62	388.87	416.05	81.77	342.07	0.29	3.66E-04
400	IMR	326.03	271.86	282.67	105.13	76.97	0.99	9.51E-04
400	Gleeble	286.88	269.34	280.03	64.83	92.24	0.51	5.22E-04
450	Gleeble	211.01	199.53	203.66	57.31	47.64	0.48	4.90E-04
500	IMR	161.31	124.36	136.59	42.52	34.55	0.65	9.12E-04
500	Gleeble	146.41	112.30	128.27	22.07	41.29	0.60	7.39E-04
550	Gleeble	114.55	99.57	107.08	35.90	30.67	0.42	5.34E-04
600	IMR	94.16	73.23	70.87	23.61	34.02	0.60	9.04E-04
600	Gleeble	86.45	79.56	83.37	31.61	29.06	0.27	4.46E-04
650	Gleeble	69.28	65.74	68.35	29.85	29.76	0.22	5.03E-04
700	IMR	57.88	43.03	44.00	19.92	10.13	0.52	8.79E-04
700	Gleeble	57.65	54.04	56.72	18.54	30.47	0.19	5.23E-04
750	IMR	42.84	28.78	29.86	14.82	0.54	0.51	8.80E-04
750	Gleeble	45.21	44.27	45.14	17.93	8.97	0.18	4.95E-04
800	IMR	27.49	17.87	17.89	9.21	10.01	0.56	8.89E-04
800	Gleeble	17.48	16.24	16.76	5.88	5.26	0.09	5.43E-04

Table 8. Tensile Result Summary of High-Temperature Tensile Tests Conducted by IMR and in the Gleeble (English Units)

Temperature (°F)	Test Provider	UTS (ksi)	0.2% Yield Stress (ksi)	0.5% Yield Stress (ksi)	Elastic Modulus (Msi)	Failure Stress (ksi)	Max Strain (in/in)	Average Strain Rate (s^{-1})
68	IMR	105.88	58.63	63.13	18.03	59.17	0.34	1.69E-03
68	Gleeble	104.98	53.45	57.35	17.24	100.23	0.37	4.44E-04
212	IMR	103.01	54.07	58.55	18.05	100.27	0.31	8.43E-04
212	Gleeble	102.70	65.39	68.45	12.38	102.21	0.23	3.26E-04
392	IMR	101.83	56.27	61.89	23.60	58.24	0.29	8.61E-04
392	Gleeble	98.94	63.60	66.90	15.49	98.27	0.17	2.50E-04
572	IMR	89.38	51.73	58.58	17.90	52.13	0.25	8.28E-04
572	Gleeble	85.55	57.83	61.88	12.62	85.21	0.13	3.10E-04
662	Gleeble	67.24	56.40	60.34	11.86	49.61	0.29	3.66E-04
752	IMR	47.29	39.43	41.00	15.25	11.16	0.99	9.51E-04
752	Gleeble	41.61	39.06	40.61	9.41	13.38	0.51	5.22E-04
842	Gleeble	30.60	28.94	29.54	8.32	6.91	0.48	4.90E-04
932	IMR	23.39	18.04	19.81	6.17	5.01	0.65	9.12E-04
932	Gleeble	21.23	16.29	18.60	3.20	5.99	0.60	7.39E-04
1022	Gleeble	16.61	14.44	15.53	5.21	4.45	0.42	5.34E-04
1112	IMR	13.66	10.62	10.28	3.43	4.93	0.60	9.04E-04
1112	Gleeble	12.54	11.54	12.09	4.59	4.21	0.27	4.46E-04
1202	Gleeble	10.05	9.53	9.91	4.33	4.32	0.22	5.03E-04
1292	IMR	8.39	6.24	6.38	2.89	1.47	0.52	8.79E-04
1292	Gleeble	8.36	7.84	8.23	2.69	4.42	0.19	5.23E-04
1382	IMR	6.21	4.17	4.33	2.15	0.08	0.51	8.80E-04
1382	Gleeble	6.56	6.42	6.55	2.60	1.30	0.18	4.95E-04
1472	IMR	3.99	2.59	2.60	1.34	1.45	0.56	8.89E-04
1472	Gleeble	2.54	2.36	2.43	0.85	0.76	0.09	5.43E-04

Table 9. Condensed Flow Stress Results for Tensile Data Collected at IMR and in the Gleeble

		True Plastic Strain (mm/mm)										Max True Stress (MPa)
Test Provider	Temperature (°C)	0	0.05	0.1	0.15	0.2	0.25	0.3	0.35	0.4	Max Plastic Strain	
Gleeble	20	370.40	593.99	723.71	812.38	879.79	932.43	956.85	-	-	0.304	957.74
IMR	20	406.37	639.99	747.87	826.50	890.66	939.83	-	-	-	0.262	943.97
Gleeble	100	454.20	662.53	761.56	825.31	867.39	-	-	-	-	0.202	868.43
IMR	100	374.67	600.32	715.11	796.82	863.82	911.90	-	-	-	0.253	913.78
Gleeble	200	441.21	653.66	743.47	793.02	-	-	-	-	-	0.149	794.58
IMR	200	389.66	606.62	713.32	791.73	855.77	897.70	-	-	-	0.247	897.70
Gleeble	300	401.37	605.53	655.43	-	-	-	-	-	-	0.116	664.50
IMR	300	358.29	580.72	668.84	716.74	747.28	-	-	-	-	0.216	755.20
Gleeble	350	391.49	476.30	478.32	-	-	-	-	-	-	0.139	480.31
Gleeble	400	271.03	303.19	305.81	310.55	-	-	-	-	-	0.195	314.00
IMR	400	272.98	335.34	346.41	356.20	365.03	373.69	380.98	387.36	390.61	0.480	395.20
Gleeble	450	200.64	220.82	-	-	-	-	-	-	-	0.052	222.82
Gleeble	500	113.10	153.69	160.81	160.27	161.71	-	-	-	-	0.288	163.49
IMR	500	124.98	169.59	173.63	176.41	178.63	180.08	180.63	-	-	0.329	181.46
Gleeble	550	100.06	118.29	-	-	-	-	-	-	-	0.046	119.05
Gleeble	600	79.93	87.70	-	-	-	-	-	-	-	0.027	88.74
IMR	600	73.62	97.37	97.80	98.39	-	-	-	-	-	0.194	99.90
Gleeble	650	66.02	-	-	-	-	-	-	-	-	0.021	70.47
Gleeble	700	54.32	54.89	-	-	-	-	-	-	-	0.009	58.45
IMR	700	43.23	-	-	-	-	-	-	-	-	0.043	59.54
Gleeble	750	44.47	-	-	-	-	-	-	-	-	0.006	45.62
IMR	750	28.88	-	-	-	-	-	-	-	-	0.044	44.32
Gleeble	800	16.48	-	-	-	-	-	-	-	-	0.006	17.65
IMR	800	17.90	-	-	-	-	-	-	-	-	0.026	28.19

Table 10. Condensed Flow Stress Results for Tensile Data Collected at IMR and in the Gleeble (True Stress Values in ksi)

		True Plastic Strain (in/in)										Max True Stress (ksi)
Test Provider	Temperature (°F)	0	0.05	0.1	0.15	0.2	0.25	0.3	0.35	0.4	Max Plastic Strain	
Gleeble	68	53.72	86.15	104.96	117.82	127.60	135.23	138.78	-	-	0.304	138.90
IMR	68	58.94	92.82	108.47	119.87	129.17	136.31	-	-	-	0.262	136.91
Gleeble	212	65.87	96.09	110.45	119.70	125.80	-	-	-	-	0.202	125.95
IMR	212	54.34	87.07	103.71	115.57	125.28	132.25	-	-	-	0.253	132.53
Gleeble	392	63.99	94.80	107.83	115.01	-	-	-	-	-	0.149	115.24
IMR	392	56.51	87.98	103.45	114.83	124.11	130.20	-	-	-	0.247	130.20
Gleeble	572	58.21	87.82	95.06	-	-	-	-	-	-	0.116	96.37
IMR	572	51.96	84.22	97.00	103.95	108.38	-	-	-	-	0.216	109.53
Gleeble	662	56.78	69.08	69.37	-	-	-	-	-	-	0.139	69.66
Gleeble	752	39.31	43.97	44.35	45.04	-	-	-	-	-	0.195	45.54
IMR	752	39.59	48.64	50.24	51.66	52.94	54.20	55.25	56.18	56.65	0.480	57.32
Gleeble	842	29.10	32.03	-	-	-	-	-	-	-	0.052	32.32
Gleeble	932	16.40	22.29	23.32	23.24	23.45	-	-	-	-	0.288	23.71
IMR	932	18.13	24.60	25.18	25.59	25.91	26.12	26.20	-	-	0.329	26.32
Gleeble	1022	14.51	17.16	-	-	-	-	-	-	-	0.046	17.27
Gleeble	1112	11.59	12.72	-	-	-	-	-	-	-	0.027	12.87
IMR	1112	10.68	14.12	14.18	14.27	-	-	-	-	-	0.194	14.49
Gleeble	1202	9.58	-	-	-	-	-	-	-	-	0.021	10.22
Gleeble	1292	7.88	7.96	-	-	-	-	-	-	-	0.009	8.48
IMR	1292	6.27	-	-	-	-	-	-	-	-	0.043	8.64
Gleeble	1382	6.45	-	-	-	-	-	-	-	-	0.006	6.62
IMR	1382	4.19	-	-	-	-	-	-	-	-	0.044	6.43
Gleeble	1472	2.39	-	-	-	-	-	-	-	-	0.006	2.56
IMR	1472	2.60	-	-	-	-	-	-	-	-	0.026	4.09

This page intentionally left blank

DISTRIBUTION

EXTERNAL

	Copies
DEFENSE TECHNICAL INFORMATION CENTER 727 JOHN J KINGMAN ROAD SUITE 0944 FORT BELVOIR, VA 22060-6218	1
RESEARCH COMMONS NAVAL UNDERSEA WARFARE CENTER BUILDING 101 NEWPORT, RI 02841	1
CHIEF OF NAVAL RESEARCH ATTN: CODE 332 OFFICE OF NAVAL RESEARCH 875 NORTH RANDOLPH STREET ARLINGTON VA 22217 ATTN: Farren, Mullins, Wolk	3
COMMANDER ATTN: SEA 05P2 NAVAL SEA SYSTEMS COMMAND 1333 ISAAC HULL AVENUE S.E. WASHINGTON NAVY YARD WASHINGTON, DC 20376 ATTN: Archer, Bjornson, McGrorey, Melvin	4
COMMANDER ATTN: SEA 05P4 NAVAL SEA SYSTEMS COMMAND 1333 ISAAC HULL AVENUE S.E. WASHINGTON NAVY YARD WASHINGTON, DC 20376 ATTN: Rodgers	1
COMMANDER ATTN: Code 6356, 6394 US NAVAL RESEARCH LABORATORY 4555 OVERLOOK AVE SW WASHINGTON, DC 20375 ATTN: Birnbaum, Iliopoulos, Michopoulos, Rowenhorst, Steuben, Stewart	6
OHIO STATE UNIVERSITY WELDING ENGINEERING PROGRAM 1248 ARTHUR E ADAMS DR COLUMBUS, OH 43221 ATTN: Fink	1

NSWCCD INTERNAL DISTRIBUTION

Code	Name	Copies
60		1
60	Mercier	1
60	Rivera	1
60	Hovanec	1
604	Waters	1
61	DeLoach	1
611	Davis	1
611	Bechetti	1
611	Dantin	1
611	Fisher	2
611	Le	1
611	Norkett	1
611	Semple	1
611	Sinfield	1
612	Roe	1
612	Draper	1
612	Gaies	1
618	Hopkins	1
618	Canaday	1
618	Gershen	1
618	Hovanec	1
618	Vail	1
651	Henes	1
651	Nelson	1
651	Rodriguez	1
652	Nasrin	1
652	Snyder	1
664	Miraglia	1
664	Nahshon	1


NAVSEA
WARFARE CENTERS
Carderock